The Error Performance of Space-Time Codes over MIMO Millimeter-Wave Channels: Design Criteria and New Insights

A Thesis

Presented in Partial Fulfillment of the Requirements for the

Degree of Master of Science

with a

Major in Electrical Engineering

in the

College of Graduate Studies

University of Idaho

by

Ahmed Aboutaleb

Major Professor: Zouheir Rezki, Ph.D.

Committee Members: Dennis Sullivan, Ph.D.; Lyudmyla Barannyk, Ph.D.

Department Administrator: Mohsen Guizani, Ph.D.

May 2018

Authorization to Submit Thesis

This thesis of Ahmed Aboutaleb, submitted for the degree of Master of Science with a major in Electrical Engineering and titled "The Error Performance of Space-Time Codes over MIMO Millimeter-Wave Channels: Design Criteria and New Insights", has been reviewed in final form. Permission, as indicated by the signatures and dates given below, is now granted to submit final copies to the College of Graduate Studies for approval.

Major Professor: _____Date_____
Zouheir Rezki, Ph.D.

Committee Members: _____Date_____
Dennis Sullivan, Ph.D.

_____Date_____
Lyudmyla Barannyk, Ph.D.

Department Administrator: _____Date_____
Mohsen Guizani, Ph.D.

Abstract

This thesis considers the error performance limits of millimeter-wave communication systems. To derive such performance limits, an accurate statistical channel model must be developed. We argue that the Nakagami-m distribution accurately models the statistics of small-scale fading at millimeter-wave-wave frequencies and provide extensive numerical simulations for the indoor environment at 60 GHz. Then, we derive an upper bound on the error performance of any space-time coding scheme that well-describes the diversity and coding gains. Our upper bound is based on the pairwise error probability (PEP). We examine the resulting diversity and coding gains to propose design criteria and desirable properties for space-time codes to maximize these gains. This results in new interesting properties that apply specifically to Nakagami-m fading channels and not necessarily to Rayleigh and Rician fading channels. We show that orthogonal space-time block codes achieve the maximum diversity gain but not the maximum coding gain. Indeed, we show that there exists a trade-off between the diversity gain and the coding gain.

In addition, we investigate the effect of blockage on the error performance using stochastic geometry. Our analysis and simulations show that blockage only reduces the coding gain and does not affect the diversity gain. This reduction in the coding gain is a function of the probability of a line-of-sight communication, path loss exponents, the distance between transceivers, and the coding gain without considering the effect of blockage. For instance, in a typical indoor environment for millimeter-wave communication, blockage due to humans or other obstacles can reduce the coding gain by up to 1.5 dB for a bit error probability of 10^{-3}.

Acknowledgements

I would like to deeply thank my advisor, Dr. Rezki, for his close supervision of this work and of my studies. Without his guidance, this research would not have been possible. I am very impressed by his rigorous and comprehensive approach to research problems. I learned from him how to be a better researcher. For that, I am indebted to him.

I would also like to thank the committee members, Prof. Sullivan and Prof. Barannyk, for kindly volunteering their time and efforts to improve thesis.

I would also like to thank the ECE department administration, Dr. Guizane, Mollyann Jones, and Stephanie Bunney, for their continued help with all the logistics involved with courses, contracts, and the submission of this thesis. I am also thankful to Kathy Duke at the College of Graduate Studies for reviewing the format of this manuscript.

I would also like to thank the friends I made during my time at the University of Idaho: Mohannad, Mustafa, Morteza, Syrine, Taha, Wael, Parvis, and Richard. Their companionship made this journey more enjoyable.

Finally, I would like to thank my mother, Mona, for her encouragement and support throughout my life and in particular during the last two years. Without her sacrifices, I would never have been able to reach this stage in life. I am also thankful to my sister, Yasmin, and my brother, Yousef, for their continued encouragement.

Table of Contents

Authorization to Submit Thesis ..... **ii**

Abstract ..... **iii**

Acknowledgements ..... **iv**

Table of Contents ..... **v**

List of Tables ..... **vii**

List of Figures ..... **viii**

1 Introduction and Background **1**

1.1 Motivation 1

1.2 Channel Modeling 3

1.3 PEP over Nakagami-m Fading Channels 5

1.4 Contribution 7

1.5 Notation 8

2 Modeling the Statistics of Small-Scale Fading **10**

2.1 Statistical Model 10

2.2 The CTF from Geometry and Properties of The Environment 11

2.3 Simulation of the Statistics of Multipath Fading for Indoor Environments 12

3 Error Performance Analysis **16**

3.1 System Model and Related Background 16

3.2 Statistics of the Envelope of a Linear Combination of Complex Nakagami-m Variables 19

3.3 Upper Bound on PEP under Nakagami-m Fading for MIMO Systems 21

3.4 Design Criteria 23

4 Effect of Blockage on the Average PEP 27

4.1 Preliminaries 27

4.2 Average PEP 28

4.3 Expressing P_{LOS} as a Function of Environmental Properties 29

4.4 Numerical Results 31

5 Conclusions and Future Works 35

Appendix A: Normalization Convention. 37

Appendix B: Proof of PDF of $\beta_{i,j}$. 38

Appendix C: Proof of Proposition 1: The Bounds on the Coding Gain 39

Appendix D: Evaluating the probability of blockage due to heights and radii of obstacles 40

List of Tables

1.1 Comparison between spectrum and data rates of cellular standards. 3

2.1 Shows the parameters of distributions used to fit CDF of $|H(f)|$ and the mean squared error for between each CDF fit and ECDF. 15

3.1 Differences between our proposed design criteria and the criteria in [1]. 23

List of Figures

1.1 Shows diverse multipath components of a transmitted signal traveling from the transmitter (Tx) to the receiver (Rx). 4

1.2 The progression of ideas in this thesis. 6

2.1 Comparison of common CDF fits to the amplitude and phase of the CTF for our proposed method and model in [2]. 14

3.1 A typical MIMO system. 17

4.1 A blockage event. 28

4.2 Error performance versus SNR for space-time block codes under different Nakagami-m fading channel conditions and blockage considerations. 31

4.3 BER versus SNR for space-time block codes under different Nakagami-m fading channel conditions and blockage considerations. 32

CHAPTER 1

Introduction and Background

1.1 Motivation

Wireless communication is possible partly due to the standardization of protocols used by transmitters and receivers over certain frequency bands. These protocols have evolved to satisfy new user requirements and allow for more utilities. The services, data dates, and spectrum of different wireless standards are summarized in Table 1.1. The first generation (1G) standard relied on analog communication and was implemented in the 1980s [3]. The services provided via the 1G standard were limited to voice communication only. Analog communication systems however have proved to be inefficient in terms of capacity and precluded the implementation of digital coding techniques [4, pp. 190]. This motivated the development of the second generation (2G) cellular standard. This new standard was implemented during the 1990s and allowed for using digital modulation and coding techniques. Further, 2G introduced the short messaging service (SMS) and provided low data rates of Internet access over the frequency spectrum 150 MHz – 450 MHz [4, pp. 187].

The popularity of the services provided by 2G initiated a revolution in cellular communication, but 2G was deficient in two main ways. First, the low data rates (25–64 kilobits per second (kbps) per user) supported by 2G prevented the development of mobile applications that require high Internet speeds for real-time interaction. Second, 2G did not support transmit diversity techniques that required channel state information at the receiver only (CSI-R), where diversity here is in terms of having different propagation paths between the transmitter and receiver as shown in Fig. 1.1. Transmit diversity techniques are signal processing methods that improve reliability and capacity through increasing the number of transmit antennas [5, pp. 253–260]. Transmit diversity was at the time more important than receive diversity because base stations could be packed with a high number of transmit antenna, while the small-size of hand-held mobile phones restricted the number of antennas that could

be equipped at the receiver [5, pp. 114]. Fortunately, in 1998, Alamouti [6] proposed the first space-time code that achieves transmit diversity while requiring only CSI-R.

To overcome the limitations of 2G, the third generation (3G) wireless standard was developed and implemented during 2000s. 3G allowed for higher data rates of up to 2 megabits per second (Mbps) [4, pp. 193]. In addition, 3G used the concepts from the Alamouti coding scheme to achieve transmit diversity, improving rate and reliability. Moreover, code-division multiple-access (CDMA) techniques were incorporated in 3G standards to increase spectral efficiency (a measure of the efficiency of utilizing the available bandwidth) [3]. The demand for higher data rates further motivated the evolution of 3G into long-term evolution (LTE), which in turn could reach data rates of up to 20 Mbps. Due to an increase in the need for even higher Internet speeds, more coverage, and improved quality of service, fourth generation (4G) wireless standards were ultimately developed and deployed around 2013. 4G used multiple antennas techniques such as spatial multiplexing and beam forming to further increase spectral efficiency, allowing theoretical data rates of up to 100 Mbps. However, the current 700 MHz – 2.6 GHz spectrum did not anticipate the high number of users today communicating using the 4G standard. This scarcity of the spectrum lead to data rates that are much lower than the expected theoretical rates and hindered the evolution of the cellular standard. As a result, to continue improving data rates and quality of service, more spectrum is required [3].

Communicating via the fifth generation (5G) standard is expected to occur also at wireless millimeter-wave frequencies (30 GHz – 100 GHz), as opposed to only communicating over the 700 MHz – 2.6 GHz bandwidth in previous and current standards [7]. This massive expansion in bandwidth promises alleviating spectrum scarcity and providing high data rates to users [3,7,8]. Further, the Federal Communications Commission (FCC) publicly recognizes that communicating over the millimeter-wave spectrum could support an increased number of users through spectrum reuse – which is possible due to the directivity of the channel and the high frequency communication resulting in reduced-size, smart antenna arrays [9]. Thus,

Table 1.1: Comparison between spectrum and data rates of cellular standards.

Standard	Services	Speeds	Spectrum
1G	-Voice Communication	0 kbps	150 MHz – 450 MHz
2G	-Voice Communication -SMS -Low Data Rate Internet Access	Up to 64 kbps	150 MHz – 450 MHz
3G	-Voice Communication -SMS -Moderate Data Rate Internet Access	Up to 20 Mbps	700 MHz – 2.6 GHz
4G	-Voice Communication -SMS -High Data Rate Internet Access	Up to 100 Mbps	700 MHz – 2.6 GHz
5G	-Voice Communication -SMS -Very High Data Rate Internet Access	1-2 Gbps	700 MHz – 2.6 GHz 30 GHz – 300 GHz

this high potential for the millimeter-wave spectrum to revolutionize cellular communication is why the community is highly interested in modeling and understanding the performance limits of the millimeter-wave channel, such as [2, 3, 7–18].

1.2 Channel Modeling

Reliable communication over the millimeter-wave channel requires accurate models of the wireless channel. These models may differ from conventional radio frequency (RF) channel models. In [16], the authors propose a statistical method for modeling wireless channels at 60 GHz. Due to the high frequency propagation over the millimeter-wave channel, propagating waves experience a very high path loss, resulting in a reduced randomness of scattered and diffracted waves arriving at the receiver. The statistical model [16] exploits this reduced random nature of the millimeter-wave channel to model the channel using only properties of the environment, the statistics of the transmitter's and receiver's locations, and ray tracing. But, it turns out that this method is too computationally demanding since it computes distributions of virtual sources' (VSs) locations before using Monte Carlo (MC) simulations to calculate the channel coefficients. On the other hand, the authors in [18] propose a more

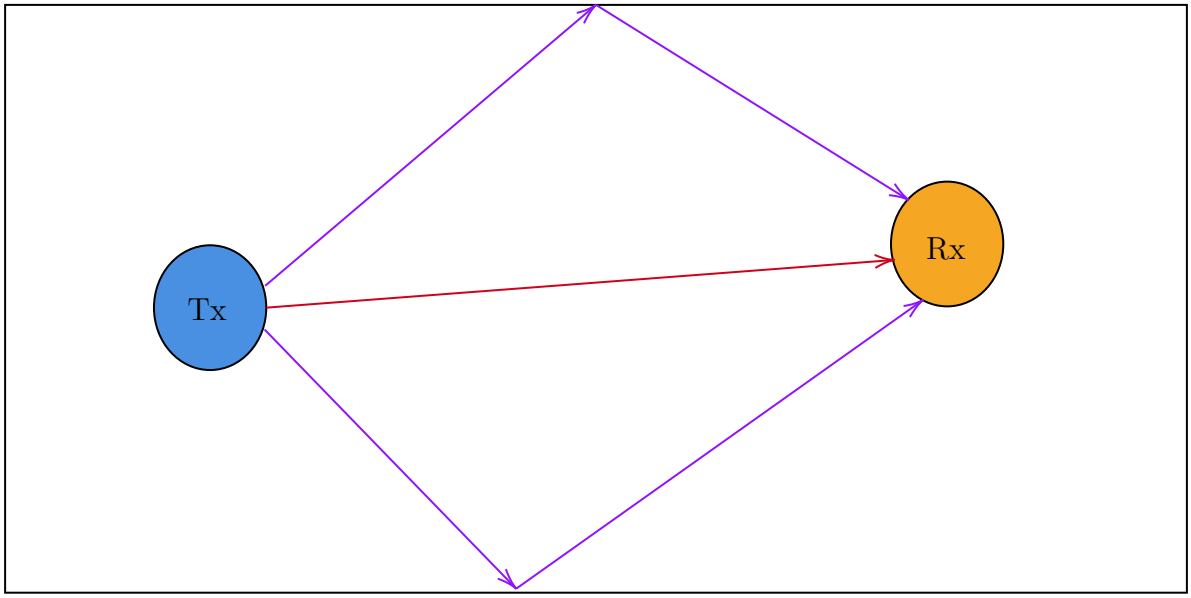

Figure 1.1: Shows diverse multipath components of a transmitted signal traveling from the transmitter (Tx) to the receiver (Rx).

computationally efficient method for modeling the millimeter-wave wireless channel than the method proposed in [16]. The authors in [18] published their method in an open source software program tailored as millimeter-Trace. While the proposed model in [18] allows for investigating interference at millimeter-wave frequencies when having multiple transceivers, their proposed model is only two-dimensional. A model for the millimeter-wave channel needs to be three-dimensional to be useful for applications involving smart antennas [16]. In [2], an experimental investigation for indoor channel at 60 GHz for a conference room is proposed, which contrast with the geometry-based approaches (that use environment properties and ray-tracing rather that measurements) in [16, 18].

Closed-form expressions for the statistics of the wireless channel also allow for accurate and intuitive assessment of its performance limits. For instance, statistical models of the channel have been used used to analyze performance metrics of the millimeter-wave channel such coverage probability, outage probability, and error probability in [10, 11, 13, 14]. In [10] and [11], the authors analyze the coverage probability for millimeter-wave cellular networks assuming the channel coefficients that model small-scale fading are Nakagami-m-distributed.

But in [13] and [14], the error and outage performances of millimeter-wave relaying channels are analyzed assuming Rayleigh and Rician small-scale fading coefficients, respectively. Moreover, the seminal works by Tarokh *et al.* [1, 19] analyze the error performance of space-time codes over Rayleigh and Rician fading channels. However, the Nakagami-m distribution has been shown to accurately model the statistics of small-scale fading (i.e., channel gains) for various channels [10, 20–23], including the millimeter-wave channel [10, 23].

1.3 PEP over Nakagami-m Fading Channels

Analytical expressions for the statistics of the channel allow for establishing clear design criteria for space-time codes to achieve the maximum diversity and coding gains of the channel. In the seminal work of Tarokh *et al.* [1], design criteria for multiple-input-multiple-output (MIMO) Rician and Rayleigh fading channels were proposed from derivations of the average pairwise error probability (PEP). Although the PEP for single-input-single-output (SISO) and single-input-multiple-output (SIMO) systems under Nakagami-m fading channels is known and can be easily derived, efforts to characterize the average PEP over Nakagami-m fading channels for MIMO communication systems have been less successful. The reason, as will be discussed in detail in Section 3.2, is the lack of a tractable, closed-form expressions for the exact distribution of the amplitude of the sum of complex-valued, Nakagami-m-distributed random variables. In [24] and [25], exact expressions of the PEP over Nakagami-m fading MIMO channels are proposed in terms of an infinite series and integral forms, respectively. These exact expressions, however, preclude the deduction of diversity and coding gains and inference of design criteria as performed in [1] for Rayleigh and Rician fading channels.

Finally, the known directivity of the millimeter-wave channel makes blockage an even more significant phenomenon that needs incorporating into any model and analysis of the wireless channel [3, 8, 10, 11, 26, 27]. In [26], a framework for analyzing performance metrics for millimeter-wave cellular networks using stochastic geometry is proposed. In [10] and [11],

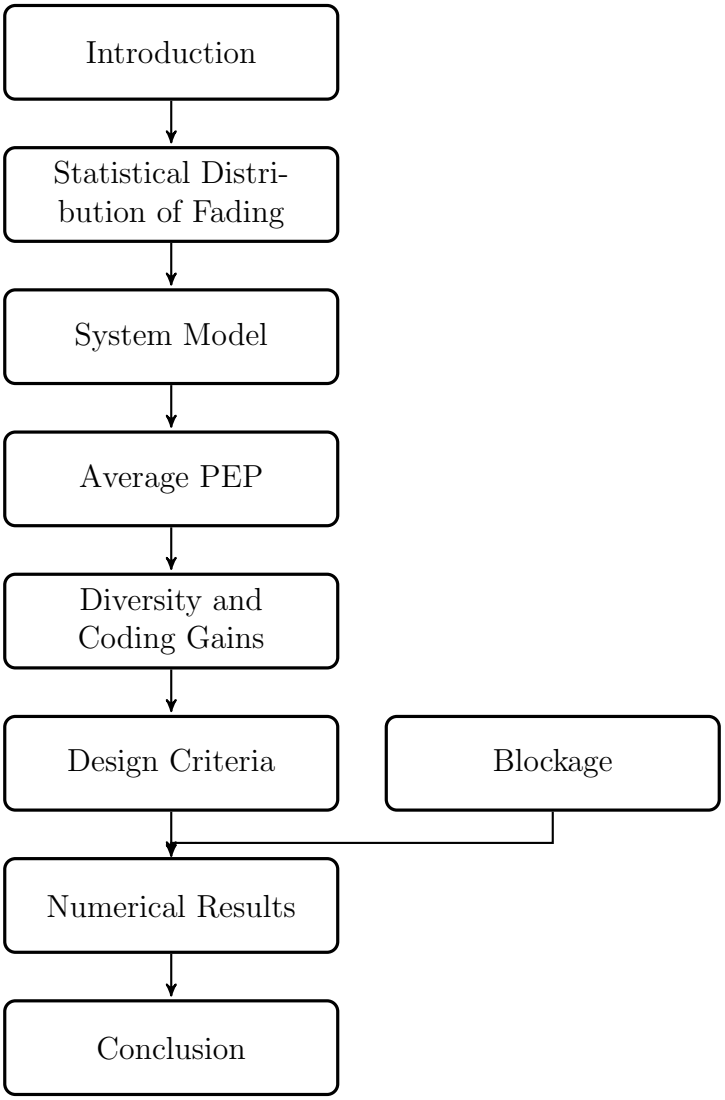

Figure 1.2: The progression of ideas in this thesis.

objects that can cause blockage are modeled using a Poisson point process (PPP) with a certain density that is considered to be a system parameter. Using stochastic geometry, the Thinning Theorem can then be invoked [28] to obtain effective densities of obstacles that can cause blockage (also known as densities of obstacles in the blocking region). For instance, in [10] and [11], this method is used to derive and analyze outage and coverage probabilities for millimeter-wave cellular networks. In [27], stochastic geometry is used to analyze the capacity of millimeter-wave networks. In [29], the authors derive the rate and coverage probability for outdoor cellular networks using a ball-based blockage model. However, the

effect of blockage on the PEP and the diversity and coding gains has not been investigated.

1.4 Contribution

This thesis in mainly comprised of our works in [22, 30]. The structure of the thesis is summarized in Fig. 1.2. In the thesis, we derive design criteria for space-time codes used over the millimeter-wave channel. Our contributions can be summarized as follows.

1. We modify the method in [16] to model the statistics of small-scale fading at 60 GHz for the indoor channel in a computationally efficient way. That is, we sample from assumed distributions of transceivers' locations; compute locations of prominent virtual sources for each sample using ray-tracing; and then compute the empirical channel transfer function (CTF). We identify the Nakagami-m cumulative distribution function (CDF) to closely match the obtained empirical cumulative distribution function (ECDF) of the CTF. We also compare the statistics of small-scale fading obtained using our approach with the measurements-based, statistical method in [2], thus, confirming that the Nakagami-m distribution is a good statistical channel model for indoor millimeter-wave communication systems.

2. To gain insights into fundamental error-performance limits of millimeter-wave channels, we derive an upper bound on the error performance for any space-time code over Nakagami-m fading MIMO channels that well-characterizes the diversity and coding gains. Our upper bound is based on the PEP. To this end, we use a result by Nakagami in [20] to obtain a closed-form expression for the sum of complex Nakagami-m-distributed random variables. We then infer design criteria for space-time codes to maximize the achievable diversity and coding gains from the derived PEP expression. Further, we show that the **determinant criterion** for space-time codes in [1] does not necessarily lead to the maximum coding gain. But, for space-time codes with a certain symmetrical property, the well-known **determinant criterion** shows up. Moreover,

we show that there is a trade-off between the diversity and coding gains for space-time codes communicating over Nakagami-m fading channels.

3. We use stochastic geometry to study the effect of blockage, due to objects in indoor environments, on the error performance of millimeter-wave communication systems. We show that the diversity gain is unaffected by blockage but the coding gain in presence of blockage is reduced, with the reduction being a function of the probability of line-of-sight (LOS) communication, power loss exponents, the distance between transceivers, and the coding gain without considering the effect of blockage.

Note that research works such as [24, 25, 31] analyze the PEP for MIMO, Nakagami-m fading channels but provide integral forms of the average PEP over the channel fading, which precludes inference of design criteria as in [1] for Rician and Rayleigh fading channels. To the best of the authors' knowledge, there has been no previous works on deriving design criteria for space-time codes communicating over MIMO, Nakagami-m fading channels (contribution 2). Furthermore, Previous studies, such as [10, 11, 13, 14, 26, 27, 29], have used stochastic geometry to derive the coverage probability and capacity for millimeter-wave channels. But, to the best of the authors' knowledge, there has been no research on the error performance of space-time codes over the millimeter-wave channel that considers blockage (contribution 3).

1.5 Notation

We represent an arbitrary $N \times M$ matrix $\mathbf{A}$ with complex entries $a_{i,j}$ by $\mathbf{A} = [a_{i,j}] \in \mathbb{C}^{N \times M}$. The square of the Frobenius norm of an arbitrary matrix $\mathbf{A} = [a_{i,j}] \in \mathbb{C}^{N \times M}$ is defined as $\|\mathbf{A}\|_F^2 = \mathrm{tr}(\mathbf{A}^H \mathbf{A}) = \sum_{i=1}^{N} \sum_{j=1}^{M} |a_{i,j}|^2$, where $\mathrm{tr}(\mathbf{A})$ represents the trace of $\mathbf{A}$, and $\mathbf{A}^H$ denotes the Hermitian of $\mathbf{A}$. We denote the Euclidean norm of a real-valued vector $\mathbf{r} \in \mathbb{R}^{N \times 1}$ by $\|\mathbf{r}\|_2$. $\Pr\{\zeta\}$ denotes the probability measure over some sample space Ω of a subset $\zeta \subset \Omega$. We represent a random variable by an uppercase letter, e.g., X, its realization by a

lowercase letter, e.g., x, and its probability density function (PDF) by $f_X(x)$. $\mathbb{E}_Y\{\cdot\}$ denotes the expectation of the expression inside the braces over random variable Y; we omit the subscript when the expectation is taken over all random variables inside the braces. We represent a random variable X that is Nakagami-m-distributed with parameters m and Ω by $X \sim \text{Nakagami}(m, \Omega)$, where for $m \geq 1/2$ and $\Omega > 0$ the Nakagami-m PDF is defined as [20]:

$$f_X(x) = \begin{cases} 2\left(\frac{m}{\Omega}\right)^m \frac{1}{\Gamma(m)} x^{2m-1} e^{-\frac{m}{\Omega}x^2} & x \geq 0, \\ 0 & \text{otherwise}, \end{cases} \tag{1.1}$$

where $\Gamma(\cdot)$ is the Gamma function. We represent a random variable Y that is uniformly distributed over an interval $(a, b) \subset \mathbb{R}$ by $Y \sim U(a, b)$. We denote the amplitude and phase of a complex number $h \in \mathbb{C}$ by $|h|$ and $\angle h$, respectively. We use the equal sign $\doteq$ as in $f(x) \doteq g(x)$ to denote that $\lim_{x\to\infty} f(x)/g(x) = 1$.

CHAPTER 2

Modeling the Statistics of Small-Scale Fading

2.1 Statistical Model

We are interested in modeling the statistics of multipath fading in millimeter-wave bands. When different multipath components arrive at the receiver at different times, they produce a random pattern of constructive and destructive interference called multipath fading [32]. Multipath fading changes fast enough to cause bit errors during communication over time-scales that are short enough so they cannot be dealt with efficiently at a protocol level. Hence, as in [1, 5, 19, 33], only the statistics of small-scale fading are used for the error analysis of space-time codes. Modeling power loss and shadowing over the millimeter-wave channel has been extensively studied in [8] and the references therein and can be used for network-level analysis.

The author [16] models small-scale fading for the millimeter-wave channel using ray-tracing and PDFs that describe the propagation paths and amplitudes of received waves. This geometry-based approach for modeling channels contrasts with measurements-based models. Measurements-based models assume the channel is random enough in a sense that inferring the channel statistics from measurements provides a good model for the channel in general [16]. But the millimeter-wave channel lacks this randomness due to the high loss in energy experienced by traveling waves resulting from the high (GHz) frequency propagation. As a result, the millimeter-wave channel model depends mainly on environmental properties. Furthermore, the PDF of multipath amplitudes can be computed from Friis's transmission equation, given the PDF of locations of VSs and environmental properties (such as room geometry, dielectric constants of wall material, signaling frequency, etc.). The properties of the environment are assumed to be known and the distribution of VSs $\mathbf{R}_k$ is computed from distributions of transceivers' locations using the law of total probability. Let $f(\mathbf{r}_k)$ denote

the PDF of the random variable $\mathbf{R}_k$. Then, using the law of total probability,

$$f(\mathbf{r}_k) = \int_{\mathbf{A}} \int_{\mathbf{R}_{\mathrm{Rx}}} \int_{\mathbf{R}_{\mathrm{Tx}}} f(\mathbf{r}_k|\mathbf{r}_{\mathrm{Tx}}, \mathbf{r}_{\mathrm{Rx}}, \mathbf{a}) f(\mathbf{r}_{\mathrm{Tx}}) f(\mathbf{r}_{\mathrm{Rx}}) f(\mathbf{a}) d\mathbf{r}_{\mathrm{Tx}} d\mathbf{r}_{\mathrm{Rx}} d\mathbf{a}, \tag{2.1}$$

where $f(\mathbf{r}_{\mathrm{Tx}})$ and $f(\mathbf{r}_{\mathrm{Rx}})$ are the PDFs of the transmitter and receiver locations, respectively; $p(\mathbf{a})$ is the PDF of a three-dimensional vector $\mathbf{A}$ whose components are uniformly distributed over the whole three-dimensional room; and $f(\mathbf{r}_k|\mathbf{r}_{\mathrm{Tx}}, \mathbf{r}_{\mathrm{Rx}}, \mathbf{a})$ is the conditional PDF of having a virtual source at location $\mathbf{r}_k$ given the transmitter and receiver are located at positions $\mathbf{r}_{\mathrm{Tx}}$ and $\mathbf{r}_{\mathrm{Rx}}$, respectively, and given $\mathbf{a}$ [16].

The main disadvantage of modeling the millimeter-wave channel using the modeling approach in [16] is the complexity involved in computing (2.1). Note that (2.1) is an integral over three random vector, $\mathbf{A}$, $\mathbf{R}_{\mathrm{Rx}}$, and $\mathbf{R}_{\mathrm{Tx}}$, each being three dimensional. So, it is equivalent to taking nine integrals. The time required to compute integrals using most numerical integration methods grows exponentially with the number of integrals that needs to be evaluated [34]. After finding the distribution of $\mathbf{r}_k$, we would still have to use Friis's transmission equation to relate the distance traveled by waves and the geometrical properties of an environment with the channel response. Then, we would need to find the PDF of the CTF as a function of random variable $\mathbf{r}_k$. To ameliorate the computational complexity, we use MC simulations to directly obtain the statistics of the CTF.

2.2 The CTF from Geometry and Properties of The Environment

First, the PDFs of the transceivers' locations are specified as in [16]. Then, rather than evaluating (2.1) which is computationally prohibitive, we sample locations of transceivers from their assumed distributions. Samples of transceivers' locations along with the room geometry dictate the positions of VSs. From simple geometry, ray-tracing can compute the distance traveled by waves as they propagate from the transmitter to the receiver. This distance, along with environmental properties, can then be used to find the CTF. For M rays

traveling from transmitter to receiver, the transfer function $H(f)$ is sum of the contributions of each ray. Let $\mathbf{R}_i$ be a random three-dimensional vector containing the distance traveled along each axis from transmitter to the receiver. Then, $H(f)$ at the receiver is given by:

$$H(f) = \sum_{i=1}^{M} \frac{c\sqrt{G_{\text{Tx}}G_{\text{Rx}}}C_{\text{Rx}}(\theta,\psi)}{4\pi f\|\mathbf{R}_i\|_2} \prod_{j=1}^{l_{\max}} F(\theta_{i,j})C_{\text{Tx}}(\theta,\psi)\exp(-j\frac{2\pi f}{c}\|\mathbf{R}_i\|_2), \tag{2.2}$$

where f is the signaling frequency; c is the speed of light; G_{Tx} and G_{Rx} are the antennas' gains at the transmitter and receiver, respectively; C_{Tx} and C_{Rx} are the radiation patterns at the transmitter and receiver, respectively; $F(\theta_{i,j})$ is Fresnel's reflection coefficient; and $l_{\max}$ is the number of the maximum possible reflected rays [16]. Evaluating the CTF in (2.2) requires finding the distance $\|\mathbf{R}_i\|_2$ traveled by each wave. Here, instead of computing the PDF of $\|\mathbf{R}_i\|_2$, we use ray-tracing to find locations of virtual sources. VSs are virtual transmitters of reflected rays arriving at the receiver. So, the distance traveled by a wave can be computed as the distance traveled from the source to the VS's location plus distance traveled from the VS's location to the receiver. To account for amplitude attenuation and phase shift due to reflections off walls of a room, we compute Fresnel's reflection coefficients for each ray. Then, using parameters of the environment and $\|\mathbf{R}_i\|_2$, we compute a sample of $H(f)$ from (2.2). The process then repeats until enough samples are obtained to generate an empirical distribution. Algorithm 1 summarizes the procedure for generating the statistics of $H(f)$.

2.3 Simulation of the Statistics of Multipath Fading for Indoor Environments

We implemented our proposed algorithm (Algorithm 1) to find the CTF for a room of dimensions 4 m ×4 m ×4 m at a frequency of 60 GHz as in [16, 17]. For simplicity and since we are interested here in studying the statistics of the channel and not the effect of antenna gains, the antennas' gains G_{Tx} and G_{Rx} were assumed to be unity. The transceivers' locations

Algorithm 1 Proposed MC-Based Method for Obtaining the Statistics of $H(f)$

1: Assume distributions of transceivers' and obstacles' locations.
2: Sample from these distributions.
3: **for** each sample of transceivers locations **do**
4: Compute locations of virtual sources for each wall using ray-tracing described above.
5: **for** each wall in the room **do**
6: Compute angle of incidence θ.
7: Compute Fresnel's reflection coefficients.
8: **end for**
9: Sum contributions to $H(f)$ from each ray as in equation (2.2).
10: **end for**
11: Repeat steps 2 to 9 N times.
12: Compute empirical CDF of $|H(f)|$ and $\angle H(f)$. This gives us the statistics of $H(f)$.

statistics represented by $f(\mathbf{r}_{\mathrm{Tx}})$ and $f(\mathbf{r}_{\mathrm{Rx}})$ are uniformly distributed over the ceiling and over the volume between one fifth and one half the height of the room, respectively, as in [16]. Then, samples from the transmitter's and receiver's locations' distributions were used to ray-trace locations of virtual sources to compute $\|\mathbf{R}_i\|_2$. Further, for each reflected ray in the room, Fresnel's reflection coefficients were computed at each wall in the room, as is described in more detail using a ray tracing tree in [35]. The room geometry and dielectric constant of walls were acquired from [16, 17]. $H(f)$ was computed for each wave reaching the receiver using (2.2). For each order of reflected waves, five rays might possibly reach the receiver: one due to the line of sight component, and the remaining four rays are due to reflections off walls in the room. The assumption that only such a small number of rays is able to reach the receiver is due to the high power loss experienced by propagating waves due to the high propagation frequency [2, 16].

Figure 2.1 compares ECDFs of the amplitude and phase of the CTF obtained from Algorithm 1 and from the statistical model in [2] with common maximum likelihood (ML) CDF fits. In contrast with our simulated geometry-based approach, the statistical model in [2] is motivated by their experimental investigation of a conference room at 60 GHz. We

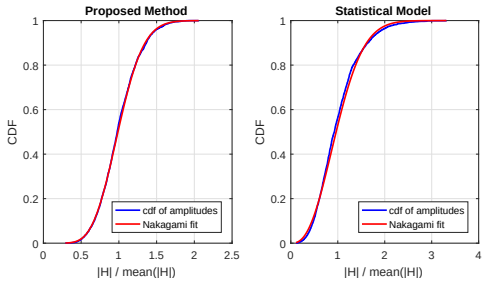

(a) A ML Nakagami-m CDF best-fit to the ECDF of the amplitude of the CTF.

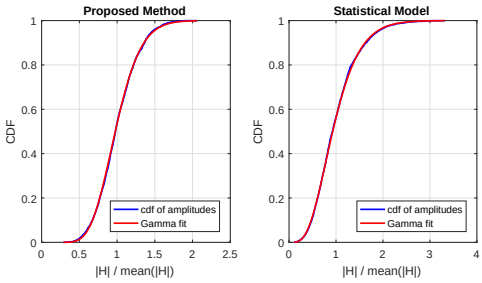

(b) A ML Gamma CDF best-fit to the ECDF of the amplitude of the CTF.

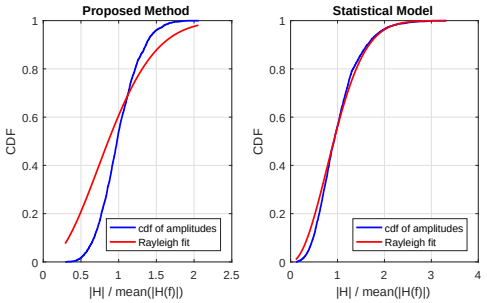

(c) A ML Rayleigh CDF best-fit to the ECDF of the amplitude of the CTF.

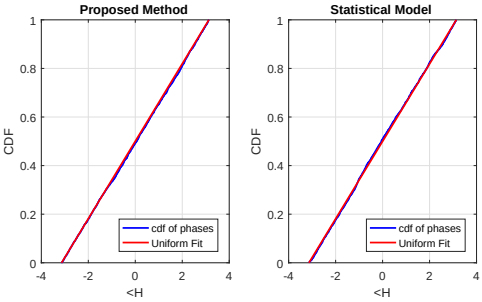

(d) A ML uniform CDF best-fit to the ECDF of the phase of the CTF.

Figure 2.1: Comparison of common CDF fits to the amplitude and phase of the CTF for our proposed method and model in [2].

are interested in finding the statistics of small-scale fading at 60 GHz for indoor environments. Figures 2.1(a) and 2.1(b) show that Nakagami-m and Gamma distributions are accurate fits for the probability distribution of the amplitude $|H(f)|$ of the CTF. This is true for both our proposed model and the statistical model in [2]. That is, for the indoor environment we considered here and in [2], the Nakagami-m distribution is a good fit for the statistics of the CTF. Figure 2.1(c) shows that the Rayleigh distribution is not a good fit for the statistics of $|H(f)|$ according to both models. Figure 2.1(d) shows that the uniform distribution between $-\pi$ and π accurately describes the statistics of the phase $\angle H(f)$ of the CTF.

We computed the mean square error (MSE) to measure how accurately a probability distribution matches the ECDF of simulated amplitudes and phases of the CTF. Table 2.1 summarizes MSE between empirical and analytic CDFs. The definitions of the distributions in Table 2.1 can be found in [36]. We find that the best CDF fits for the obtained ECDF of the amplitude are the Gamma and Nakagami-m CDFs since their maximum likelihood

Table 2.1: Shows the parameters of distributions used to fit CDF of $|H(f)|$ and the mean squared error for between each CDF fit and ECDF.

Distribution	Parameters [36]	Mean Squared Error
Gamma	$\alpha = 13.5088$, $\beta = 0.0740$	3.6006×10^{-5}
Lognormal	$\alpha =$ -0.0375, $\beta = 0.2799$	2.0427×10^{-4}
Nakagami-m	$m = 3.6350$, $\Omega = 1.0713$	1.6757×10^{-5}
Rayleigh	$\beta = 0.7319$	0.0158
Rician	$\alpha = 0.9602$, $\beta = 0.2732$	1.1934×10^{-4}
Uniform	$\alpha =$ -3.1395 , $\beta = 3.1401$	2.0427×10^{-4}
Weibull	$\mu = 1.1001$, $\Omega = 0.2105$	3.1668×10^{-4}

fits have the least MSEs, which is in order of 10^{-5}. We also observe that the distribution of phase of the CTF is approximately uniform between $-\pi$ and π. This observed uniformity of the distribution of the phase of the CTF satisfies a conjecture in the Saleh-Valenzuela model [37] which states that the phase is uniformly distributed regardless of the signaling frequency for indoor environments. Thus, we can accurately model the multipath fading statistics of the amplitude $|H(f)|$ and phase $\angle H(f)$ of the CTF in the indoor environment specified using a Nakagami-m distribution and a uniform distribution, respectively.

We showed that the amplitude and phase of multipath fading of the CTF at the millimeter-wave spectrum (at 60 GHz) in an indoor environment are accurately modeled by a Nakagami-m distribution and a uniform distribution, respectively. In the next section, we use this model to derive a general, closed-form expression for a tight upper bound on the pairwise error probability of space-time codes. Such an expression provides more insights (in terms of diversity and coding gains) into the error performance of space-time codes over millimeter-wave communication systems than numerical simulations alone.

CHAPTER 3

Error Performance Analysis

3.1 System Model and Related Background

The millimeter-wave channel is known to be wideband, but we assume a flat fading channel since any wideband channel can be split into a set of parallel narrowband channels using orthogonalization techniques [32]. Under the narrowband assumption, the realizations of the CTF are constant over all frequencies such that frequency components of transmitted signals experience the same multiplicative, complex gain. As a result, the convolution of the time-domain representation of the transmitted signal and the channel impulse response simplifies to a multiplication of the transmitted signal by a constant. We also assume the realization of the channel matrix is constant over the length of the code block (i.e., quasi-static fading), and the receiver has perfect channel state information (CSI-R). For a MIMO system, see Figure 3.1, with N_t and N_r transmit and receive antennas, respectively, and considering a block code of length T, the received symbols matrix $\mathbf{R} = [r_{i,j}] \in \mathbb{C}^{N_r \times T}$ is given by:

$$\mathbf{R} = \sqrt{\rho}\mathbf{H}\mathbf{S} + \mathbf{Z}, \tag{3.1}$$

where $\mathbf{S} = [s_{i,j}] \in \mathbb{C}^{N_t \times T}$ is the normalized transmitted symbols matrix; $\mathbf{H} = [h_{i,j}] \in \mathbb{C}^{N_r \times N_t}$ is the normalized channel matrix; $\mathbf{Z} = [z_{i,j}] \in \mathbb{C}^{N_r \times T}$ is the normalized complex additive white Gaussian noise (AWGN) matrix, i.e., $z_{i,j} \sim \mathcal{CN}(0,1)$; and $\rho \in [0, \infty)$ is the average SNR at the transmitter. (The normalization convention used is explained in Appendix A.) Each transmitted symbol $s_{i,j}$ belongs to the set of allowable alphabets $\mathcal{M}$, i.e., $s_{i,j} \in \mathcal{M}$, where $M = |\mathcal{M}|$. We define P_b as the bit error probability of the channel in (3.1). In terms of the diversity gain G_d and the coding gain G_c, P_b can be expressed as:

$$P_b = k\big\{G_c E_b/N_0\big\}^{-G_d}, \tag{3.2}$$

Figure 3.1: A typical MIMO system.

where E_b/N_0 is the bit energy to noise ratio and k is some real-valued, positive constant [33, eq. 3.19], [5, eq. (1.3)]. Unfortunately, it is difficult to compute P_b in a closed-form. However, at high SNR, a closed-form expression of the bit error probability can be obtained from an average pairwise error probability (PEP). The PEP is the probability of obtaining codeword $\mathbf{E} = [e_{i,j}] \in \mathbb{C}^{N_t \times T}$ at the receiver when codeword $\mathbf{S}$ was transmitted under channel conditions $\mathbf{H}$, at SNR ρ. Indeed, the average PEP $\Pr\{\mathbf{S} \to \mathbf{E}\}$ is itself an upper bound on the symbol error probability P_s, see [5, pp. 136-137]. But, as $\rho \to \infty$, the two error probabilities converge to the same value times a constant $c > 0$ [5, pp. 142-143], i.e., $P_s \doteq c \Pr\{\mathbf{S} \to \mathbf{E}\}$. Furthermore, for a codeword of length T and a modulation order of M, P_b is related to P_s as follows [5]:

$$P_b \doteq \frac{P_s}{T \log_2 M}. \tag{3.3}$$

Hence, in the high SNR regime, $P_b \doteq (c \ / \ T \log_2 M) \ \Pr\{\mathbf{S} \to \mathbf{E}\}$, and we can use closed-form expressions of the PEP (cf. 3.3) to obtain diversity and coding gains from (3.2). Now, assuming $\mathbf{R}$ is decoded at the receiver using a maximum likelihood decoding rule, it can be easily shown that the conditional PEP on the channel matrix is equal to [1, 5, 19]:

$$\Pr\{\mathbf{S} \to \mathbf{E}|\mathbf{H}\} = \Pr\{\|\mathbf{R} - \mathbf{HE}\|_F > \|\mathbf{R} - \mathbf{HS}\|_F\} \tag{3.4}$$

$$= Q\Big(\sqrt{\rho/2}\|\mathbf{D}\|_F\Big), \tag{3.5}$$

where $\mathbf{D} \triangleq \mathbf{H}(\mathbf{S} - \mathbf{E})$, $Q(x) = \frac{1}{\sqrt{2\pi}} \int_x^\infty \exp(-\frac{u^2}{2}) du$ is the Q-function, and $\|\mathbf{D}\|_F$ is the Frobenius norm of $\mathbf{D}$. Using the Chernoff bound on the Q-function, the conditional PEP

can be upper bounded as [5]:

$$\Pr\{\mathbf{S} \to \mathbf{E}|\mathbf{H}\} \leq \frac{1}{2}\exp\Big(\frac{-\rho\|\mathbf{D}\|_F^2}{4}\Big). \tag{3.6}$$

It can be easily shown using simple algebraic manipulations that $\|\mathbf{D}\|_F^2$ can be written as [5, pp. 138–140], [1]:

$$\|\mathbf{D}\|_F^2 = \sum_{i=1}^{N_r}\sum_{j=1}^{r}\lambda_j|\beta_{i,j}|^2, \tag{3.7}$$

where $\|\mathbf{D}\|_F^2 = \mathrm{tr}\big((\mathbf{S}-\mathbf{E})(\mathbf{S}-\mathbf{E})^H\mathbf{H}^H\mathbf{H}\big)$, $\{\lambda_j\}_{j=1}^r$ and r are the non-zero eigenvalues and rank of $(\mathbf{S}-\mathbf{E})(\mathbf{S}-\mathbf{E})^H$, respectively, and $\beta_{i,j}$ is defined as:

$$\beta_{i,j} \triangleq \sum_{j'=1}^{N_t} u_{j',j}h_{i,j'}, \tag{3.8}$$

where $\mathbf{U} = [u_{i,j}] \in \mathbb{C}^{N_t\times N_t}$ is unitary and orthogonal (i.e., $\mathbf{U}\mathbf{U}^H = \mathbf{I}$), resulting from the singular value decomposition $(\mathbf{S}-\mathbf{E})(\mathbf{S}-\mathbf{E})^H = \mathbf{U}\mathbf{\Lambda}\mathbf{U}^H$.

Hence, by substituting (3.7) into (3.6), an upper bound on the conditional PEP can be written as:

$$\begin{aligned}\Pr\{\mathbf{S} \to \mathbf{E}|\mathbf{H}\} &\leq \frac{1}{2}\exp\Big(-\frac{\rho}{4}\sum_{i=1}^{N_r}\sum_{j=1}^{r}\lambda_j|\beta_{i,j}|^2\Big)\\ &= \frac{1}{2}\prod_{i=1}^{N_r}\prod_{j=1}^{r}\exp\Big(-\frac{\rho}{4}\lambda_j|\beta_{i,j}|^2\Big).\end{aligned} \tag{3.9}$$

To get a closed-form expression for an upper bound on PEP under Nakagami-m fading, we need to average (3.9) over the channel coefficients. But diversity and coding gains derived from an upper bound on the PEP might not themselves constitute exact diversity and coding gains. Fortunately, as we show in the following lemma, the exponential bound in (3.9) is tight at high SNR.

Lemma 1: *$Q(x)$ and $\frac{1}{2}\exp(-\frac{1}{2}x^2)$ converge at the same rate and to the same value in the limit as x goes to ∞, i.e., $Q(x) \doteq \frac{1}{2}\exp(-\frac{1}{2}x^2)$.*

Proof. From [38, Theorem 1], $\alpha_1 \exp(-\beta_1 x^2)$ is an upper bound on $Q(x)$ iff $\alpha_1 \geq 1/2$ and $0 \leq \beta_1 \leq 1/2$. And, from [38, Theorem 2], $\alpha_2 \exp(-\beta_2 x^2)$ is a lower bound on $Q(x)$ if and only if $\beta_2 > 1/2$ and $0 \leq \alpha_2 \leq \sqrt{\frac{e\sqrt{\beta_2 - 1}}{2\pi\beta_2^2}}$. Taking the limit as x goes to ∞ in $Q(x)$ and its exponential bounds, and dividing by $k_1 \exp(-\frac{1}{2}x^2)$, it hence follows that:

$$\frac{\alpha_2 \exp(-\beta_2 x^2)}{\frac{1}{2}\exp(-\frac{1}{2}x^2)} \leq \frac{Q(x)}{\frac{1}{2}\exp(-\frac{1}{2}x^2)} \leq \frac{\alpha_1 \exp(-\beta_1 x^2)}{\frac{1}{2}\exp(-\frac{1}{2}x^2)}. \tag{3.10}$$

Now, in (3.10), we set $\beta_1 = 1/2$, and take the limit as β_2 and x go to $1/2$ and ∞, respectively. Thus, both the lower and the upper bounds become equal to $2\alpha_2$ and $2\alpha_1$, respectively. Now, it is permissible to set $\alpha_1 = \alpha_2 = 1/2$; making both lower and upper bounds equal to 1. Therefore, we have that:

$$\lim_{x\to\infty} \left\{ \frac{Q(x)}{\frac{1}{2}\exp(-\frac{1}{2}x^2)} \right\} = 1. \tag{3.11}$$

□

Hence, **Lemma 1** allows inferring actual diversity and coding gains from (3.9), rather than only bounds on these gains.

3.2 Statistics of the Envelope of a Linear Combination of Complex Nakagami-m Variables

We use equation (3.9) to derive an upper bound on PEP under Nakagami-m fading. Using the model of the statistics of the channel coefficients justified, we have that $|h_{i,j}| \sim$ Nakagami(m, Ω) and $\angle h_{i,j} \sim U(-\pi, \pi)$. To average the expression in (3.9), we first need to find the PDF of $|\beta_{i,j}| = |\sum_{j'=1}^{N_t} u_{j',j} h_{i,j'}|$. Note that $|\beta_{i,j}|$ can be viewed as the envelope of the sum of N_t weighted complex random variables, where the weights have a unity Euclidean

norm. Each random variable in this sum has a Nakagami-m-distributed amplitude and a uniformly distributed phase. An exact, general integral form for the PDF of the magnitude of the sum of independent, complex Nakagami-m random variables with phases that are statistically independent from amplitudes was first proposed by Nakagami [20]. Later, Du *et al.* [21] derived this integral form. Nonetheless, Nakagami [20] and Du *et al.* [21] also established that the PDF of the envelope of this sum of Nakagami-m-distributed random variables is well approximated by another Nakagami-m distribution with parameters $\widetilde{m}$ and $\widetilde{\Omega}$. Note that the problem we are considering here is the sum of complex Nakagami-m-distributed random variables. Hence, the known PDF for the sum of real Nakagami-m random variables proposed in [39], which is widely used for performance analysis of communication systems, cannot be used.

To obtain an intuitive understanding from an upper limit on the PEP in terms of the diversity gain for MIMO systems under Nakagami-m fading, we approximate the PDF of $|\beta_{i,j}|$ using a Nakagami-m distribution with parameters $\widetilde{m}$ and $\widetilde{\Omega}$ as defined in [21]. For $|h_{i,j}| \sim \text{Nakagami}(m, \Omega)$, $|\beta_{i,j}|$ is the envelope of the weighted sum of independent, complex Nakagami-m random variables, such that each term in the summation has an amplitude of $|u_{i,j}||h_{i,j}| \sim \text{Nakagami}(|u_{i,j}|^2 m, \Omega)$ and a phase of $(\angle h_{i,j} + \angle u_{i,j}) \sim U(-\pi + \angle u_{i,j}, \pi + \angle u_{i,j})$. Therefore, by applying [21, eq. (17)] (see Appendix B for more details), we have that $|\beta_{i,j}| \sim \text{Nakagami}(\widetilde{m}_j, \widetilde{\Omega})$ where:

$$\widetilde{\Omega} = \sum_{j'=1}^{N_t} |u_{j',j}|^2 \Omega = \Omega, \tag{3.12}$$

$$\begin{aligned} \widetilde{m}_j &= \frac{m}{\sum_{j'=1}^{N_t} |u_{j',j}|^4 + m \sum_{j'=1}^{N_t} \sum_{\substack{j''=1 \\ j'' \neq j'}}^{N_t} |u_{j',j}|^2 |u_{j'',j}|^2}. \\ &\overset{\text{(a)}}{=} \frac{m}{(1-m)\sum_{j'=1}^{N_t} |u_{j',j}|^4 + m}, \end{aligned} \tag{3.13}$$

where (a) follows from a simple algebraic manipulation and the fact that $\mathbf{U}$ is unitary. Note that, for the case when $m = 1$ (i.e., Rayleigh fading), $\widetilde{m}_j$ is equal to 1, i.e., the PDF of $|\beta_{i,j}|$

is Rayleigh, in agreement with [21].

The expression for $\widetilde{m}_j$ in (3.13) depends on the codeword choice through elements of matrix $\mathbf{U}$. To find bounds on $\widetilde{m}_j$ that are independent of the codeword and are useful for inferring design criteria, we bound $\sum_{j'=1}^{N_t} |u_{j',j}|^4$: $\forall u_{j',j} \in \mathbb{C}$: $\sum_{j'=1}^{N_t} |u_{j',j}|^2 = 1$, (using the Cauchy-Schwarz inequality to obtain the non-zero lower bound):

$$0 < \frac{1}{N_t} \leq \sum_{j'=1}^{N_t} |u_{j',j}|^4 \leq \sum_{j'=1}^{N_t} |u_{j',j}|^2 = 1. \tag{3.14}$$

Hence, from the inequality in (3.14), $\widetilde{m}_j$ is bounded in $\left(m, \frac{N_t m}{1+(N_t-1)m}\right]$ for $1/2 \leq m < 1$, and is bounded in $\left[\frac{N_t m}{1+(N_t-1)m}, m\right)$ for $m \geq 1$. Let $m_{\max} \triangleq \max\left(\frac{N_t m}{1+(N_t-1)m}, m\right)$ and $m_{\min} \triangleq \min\left(\frac{N_t m}{1+(N_t-1)m}, m\right)$. Therefore, the expression for $\widetilde{m}_j$ in (3.13), can be bounded according to, for $m \geq 1/2$:

$$m_{\min} \leq \widetilde{m}_j \leq m_{\max}. \tag{3.15}$$

We will find the bounds in (3.15) useful for deriving design criteria in Subsection 3.4.

3.3 Upper Bound on PEP under Nakagami-m Fading for MIMO Systems

Now that we know the PDF of $\beta_{i,j}$ and we bounded $\widetilde{m}_j$ with bounds that are independent of the codeword choice, we average the PEP over the channel statistics to obtain the diversity and coding gains. Averaging over $|\beta_{i,j}|$ in (3.9), and for $h_{i,j}$'s independent and identically distributed (i.i.d.), we obtain:

$$\begin{aligned}
&\Pr\{\mathbf{S} \to \mathbf{E}\} \\
&\leq \mathbb{E}\left\{\frac{1}{2}\prod_{i=1}^{N_r}\prod_{j=1}^{r}\exp\Big(-\frac{\rho}{4}\lambda_j|\beta_{i,j}|^2\Big)\right\}
\end{aligned}$$

$$\stackrel{(a)}{=} \frac{1}{2}\prod_{i=1}^{N_r}\prod_{j=1}^{r}\mathbb{E}\left\{\exp\Big(-\frac{\rho}{4}\lambda_j|\beta_{i,j}|^2\Big)\right\}$$
$$\stackrel{(b)}{=} \frac{1}{2}\prod_{i=1}^{N_r}\prod_{j=1}^{r}\int_0^\infty \exp\Big(-\frac{\rho}{4}\lambda_j x^2\Big)\frac{2\widetilde{m}_j^{\widetilde{m}_j}}{\Gamma(\widetilde{m}_j)\widetilde{\Omega}^{\widetilde{m}_j}}x^{2\widetilde{m}_j-1}\exp\Big(-\frac{\widetilde{m}_j}{\widetilde{\Omega}}x^2\Big)dx$$
$$\stackrel{(c)}{=} \frac{1}{2}\prod_{i=1}^{N_r}\prod_{j=1}^{r}\frac{\widetilde{m}_j^{\widetilde{m}_j}}{\widetilde{\Omega}^{\widetilde{m}_j}}\frac{1}{\big((\rho/4)\lambda_j+\widetilde{m}_j/\widetilde{\Omega}\big)^{\widetilde{m}_j}}, \tag{3.16}$$

where (a) follows from that $\beta_{i,j}$'s are functions of statistically independent random variables and are, hence, also independent (but not necessarily identically distributed); (b) follows from applying the definition of the PDF of $|\beta_{i,j}|$, $f_{|\beta_{i,j}|}(x)$; and (c) follows from that $\int_0^\infty x^n\exp(-ax^2)dx = \Gamma(\frac{n+1}{2})/\big(2a^{\frac{n+1}{2}}\big)$, for $a>0$ and $n>-1$ [40, eq. 3.326].

In the high SNR regime, $(\rho/4)\lambda_j \gg \widetilde{m}_j/\widetilde{\Omega}$, and by invoking **Lemma 1**, we can write the PEP as:

$$\begin{aligned}&\Pr\{\mathbf{S}\to\mathbf{E}\}\\ &\doteq \frac{1}{2}\prod_{i=1}^{N_r}\prod_{j=1}^{r}\frac{\widetilde{m}_j^{\widetilde{m}_j}}{\widetilde{\Omega}^{\widetilde{m}_j}}\frac{1}{\big(\lambda_j\rho/4\big)^{\widetilde{m}_j}}\\ &= \frac{1}{2}\left(\left(\prod_{j=1}^{r}\Big(\frac{\lambda_j}{\widetilde{m}_j}\Big)^{\frac{\widetilde{m}_j}{\sum_{j=1}^r\widetilde{m}_j}}\right)\frac{\widetilde{\Omega}}{4}\rho\right)^{-N_r\sum_{j=1}^r\widetilde{m}_j}.\end{aligned} \tag{3.17}$$

To deduce coding and diversity gains from (3.17), we use the definitions of the diversity G_d and coding gain G_c in (3.2). Comparing (3.17) with the definition of diversity and coding gains in (3.2), we see that the diversity and coding gains for the MIMO system in (3.1) are given by:

$$G_d = N_r\sum_{j=1}^{r}\widetilde{m}_j, \tag{3.18}$$
$$G_c = \frac{\Omega}{4}\prod_{j=1}^{r}\Big(\frac{\lambda_j}{\widetilde{m}_j}\Big)^{\frac{\widetilde{m}_j}{\sum_{j=1}^r\widetilde{m}_j}}. \tag{3.19}$$

Under Rayleigh fading ($m=1$), $\widetilde{m}_j=1$, and we retrieve the expressions for the diversity

Table 3.1: Differences between our proposed design criteria and the criteria in [1].

	Closed-Form Upper Bound	Determinant Criterion	Codes that Achieve Full Diversity	Trade-off between G_c and G_d
Tarokh *et al.* [1]	Rayleigh, Rician	Always applies	Full-rank NOSTBCs & OSTBCs.	No
This Work	Nakagami-m	Special case	OSTBCs & codes that satisfy (3.23)	Yes

and coding gains from (3.18) and (3.19) that were first derived in [1], [19], as follows:

$$G_d = rN_r,$$
$$G_c = \frac{\Omega}{4}\prod_{j=1}^{r}\lambda_j^{1/r}.$$

Assuming fading is possibly less or more severe than Rayleigh fading (i.e., $m \neq 1$), what are the bounds on the diversity and coding gains and how can optimum gains be achieved? In the next subsection, we address these questions and extend the design criteria in [1], [19] for Nakagami-m fading, MIMO channels.

3.4 Design Criteria

The fading severity under Nakagami-m fading is captured by $m \geq 1/2$. We want to find properties of space-time codes that allow for exploiting reduced fading severity to increase the diversity and coding gains. To this end, we use the bounds on $\widetilde{m}_j$ in (3.15) to bound the diversity and coding gains in (3.19), which results in the following bounds on the diversity gain G_d, for $m \geq 1/2$:

$$rN_r m_{\min} \leq G_d \leq rN_r m_{\max}. \tag{3.20}$$

Similarly, by substituting for the bounds on $\widetilde{m}_j$ in (3.19) and further analysis, the coding gain G_c satisfies the inequality in the following Proposition.

Proposition 1: *The coding gain G_c is bounded by:*

$$\frac{\Omega}{4}\prod_{j=1}^{r}\left(\frac{\lambda_j}{m_{\max}}\right)^{\frac{1}{r}} \leq G_c \leq \frac{\Omega}{4}\prod_{j=1}^{r}\left(\frac{\lambda_j}{m_{\min}}\right)^{\frac{1}{r}}. \tag{3.21}$$

Proof. For convenience, the proof is presented in Appendix C. □

For a given r, the upper bound on G_d of $rN_rm_{\max}$ is achieved if and only if $\widetilde{m}_j = m_{\max},\ \forall j = 1,\ldots,r$. Hence, for a given r, this happens if and only if $\sum_{j'=1}^{N_t}|u_{j',j}|^4 = 1,\ \forall\ j = 1,\ldots,N_t$, which gives that:

$$\begin{aligned} &\sum_{j'=1}^{N_t}|u_{j',j}|^4 = 1 \\ \overset{(a)}{\Leftrightarrow} &\sum_{j'=1}^{N_t}|u_{j',j}|^2(|u_{j',j}|^2-1) = 0, \end{aligned} \tag{3.22}$$

where (a) follows from that the Euclidean norm of rows of $\mathbf{U}$ is unity. For (3.22) to be satisfied, there are only two possible solutions: $|u_{j',j}|^2 = 0$ or $|u_{j',j}|^2 = 1$. But it is not possible that all the elements of $\mathbf{U}$ are zeros since $\sum_{i=1}^{N_t}|u_{j',j}|^2 = 1$. Thus, in every column of $\mathbf{U}$, there must be only one element whose value is unity, i.e., $\forall j = 1,2,\ldots,N_t$,

$$|u_{j',j}|^2 = \delta_{j'j_0} \triangleq \begin{cases} 1 & \text{if } j' = j_0, \\ 0 & \text{if } j' \neq j_0, \end{cases} \tag{3.23}$$

where $j_0 \in \{1,2,\ldots,N_t\}$ denotes the index of the non-zero element in each column of $\mathbf{U}$. Therefore, for a given r, space-time codes that generate a matrix $\mathbf{U}$ that is either the identity or whose columns are permutations of those of the identity matrix are the only space-time codes that achieve the maximum possible diversity gain of $rN_rm_{\max}$. Note, however, that when $\widetilde{m}_j = m_{\max},\ \forall j = 1,\ldots,r$, the lower bound on G_c in (3.21) is achieved, i.e., achieving the upper bound on G_d results in achieving the lower bound on G_c. On the other hand, the upper bound on G_c is achieved if and only if $\widetilde{m}_j = m_{\min},\ \forall j = 1,\ldots,N_t$, which occurs if and

only if $\sum_{j'=1}^{N_t} |u_{j',j}|^4 = 1/N_t$, resulting in achieving the lower bound on G_d. Hence, there is a trade-off: achieving the upper bound on G_d results in achieving the lower bound on G_c and vice versa.

Furthermore, the following design criteria hold.

- Orthogonal space-time-block codes (OSTBCs) produce a unitary matrix $\mathbf{U}$ that is the identity matrix [5, pp. 145–147], which satisfies (3.23). This follows from the definition of OSTBCs as having a matrix $\mathbf{S}$ whose rows are orthogonal. Let $\mathbf{s}_i$ denote the ith row of $\mathbf{S}$, and $\mathbf{e}_i$ denote the ith row of $\mathbf{E}$. Then, since $\mathbf{S}$ and $\mathbf{E}$ are orthogonal matrices with the same structure, the rows of $\mathbf{S}-\mathbf{E}$ are also orthogonal, i.e., $(\mathbf{s}_i - \mathbf{e}_i)(\mathbf{s}_j - \mathbf{e}_j)^H = 0$, for $i \neq j$ and $\forall i, j = 1, 2, \ldots, N_t$. As a result, the off-diagonal entries of matrix $(\mathbf{S}-\mathbf{E})(\mathbf{S}-\mathbf{E})^H$ are all zeros, and, hence, $\mathbf{U}$ is the identity. Therefore, OSTBCs satisfy (3.23) and, hence, achieve the upper bounds on G_d of $rN_r m_{\max}$.

- OSTBCs can achieve the maximum G_d in (3.20) of $rN_r m_{\max}$. Hence, designers must maximize r, the rank of $(\mathbf{S}-\mathbf{E})(\mathbf{S}-\mathbf{E})^H$, which is also known as the **rank criterion** [1].

- Since $r \leq \min(N_t, T)$, the length of the codeword T should be sufficiently large to fully exploit the benefits in terms of diversity gain due to having multiple antennas at the transmitter, i.e., $T \geq N_t$. To overcome excessive decoding delays, T must be chosen to be equal to N_t.

- Given that the upper bound on G_d is achieved, the lower bound on the G_c in (3.21) is achieved, i.e., $\widetilde{m}_j = m_{\max}\ \forall j = 1, \ldots, N_t$. To maximize this lower bound, the product of the eigenvalues $\{\lambda_j\}_{j=1}^{r}$ must be maximized (since $m_{\min}$ is independent of the codeword choice), which is also known as the **determinant criterion** [1].

- To achieve the upper bound on G_c in (3.21), we must relax the optimality constraint on G_d. Indeed, the upper bound on G_c can be achieved if and only if $\sum_{j'=1}^{N_t} |u_{j',j}|^4 = 1/N_t$, which results in $\widetilde{m}_j = m_{\min}\ \forall j = 1, \ldots, r$ in (3.19), achieving the upper bound on G_c

in (3.20) and the lower bound on G_d in (3.21). Then, the codeword must maximize the product of the eigenvalues $\{\lambda_j\}_{j=1}^{r}$ to obtain the maximum coding gain.

Remark: While, in [1], the analysis shows that the **determinant criterion** always holds for Rayleigh and Rician fading channels, this is not necessarily true for Nakagami-m fading channels. The reason is that maximizing the coding gain over Nakagami-m fading channels in (3.19) is equivalent to maximizing $\prod_{j=1}^{r}\left(\frac{\lambda_j}{\widetilde{m}_j}\right)^{\frac{\widetilde{m}_j}{\sum_{j=1}^{r}\widetilde{m}_j}}$, which is not necessarily equivalent to maximizing $\prod_{j=1}^{r}\lambda_j$ (which is the **determinant criterion**). Table 3.1 summarizes the main differences between our derived design criteria and the ones derived in [1].

CHAPTER 4

Effect of Blockage on the Average PEP

Now that we have established design criteria for space-time codes under Nakagami-m fading, we incorporate blockage into the channel model and deduce its effect on the diversity and coding gains. Blockage is a significant phenomenon to consider in highly directive channels, such as the millimeter-wave channel [3, 8, 10, 11]. To this end, we use stochastic geometry to model the statistics of obstacles in indoor environments.

4.1 Preliminaries

We use a Cartesian coordinate system xyz, where x and y are along the lengths and z is along the height of the room. We fix the locations of the transmitter and receiver at heights h_t and h_r, respectively, and at a distance d apart. Due to the assumption that the occurrence of obstacles between the transmitter and receiver follows a Poisson distributions, the distance between an obstacle and the transmitter D_0 is uniformly distributed, i.e., $D_0 \sim U(0, d)$. We assume obstacles are cylindrically-shaped with heights H_i and radii R_i that are uniformly distributed within a certain range, i.e., $H_i \sim U(h_{\min}, h_{\max})$ and $R_i \sim U(r_{\min}, r_{\max})$, where $1 \leq i \leq n$ and n is the number of obstacles between the transceivers. The number of obstacles in a room n is modeled via a PPP with density λ_b (number of obstacles per unit volume), i.e., $n \sim \text{Poisson}(\lambda_b)$ [10, 11, 28].

We model blockage as in [10], [11] using a discrete random variable $\Gamma \in [0, 1]$ that penalizes a LOS communication with probability (w.p.) P_{LOS} and a non-line of sight (NLOS) communication w.p. $1 - P_{\text{LOS}}$ as:

$$\Gamma = \begin{cases} \gamma_1 \triangleq \left(\dfrac{d}{d_{\text{ref}}}\right)^{-\alpha_{\text{L}}} & \text{w.p. } P_{\text{LOS}}, \\ \gamma_2 \triangleq \left(\dfrac{d}{d_{\text{ref}}}\right)^{-\alpha_{\text{N}}} & \text{w.p. } 1 - P_{\text{LOS}}, \end{cases} \tag{4.1}$$

where d is the distance between the transmitter and the receiver, d_{ref} is a reference distance,

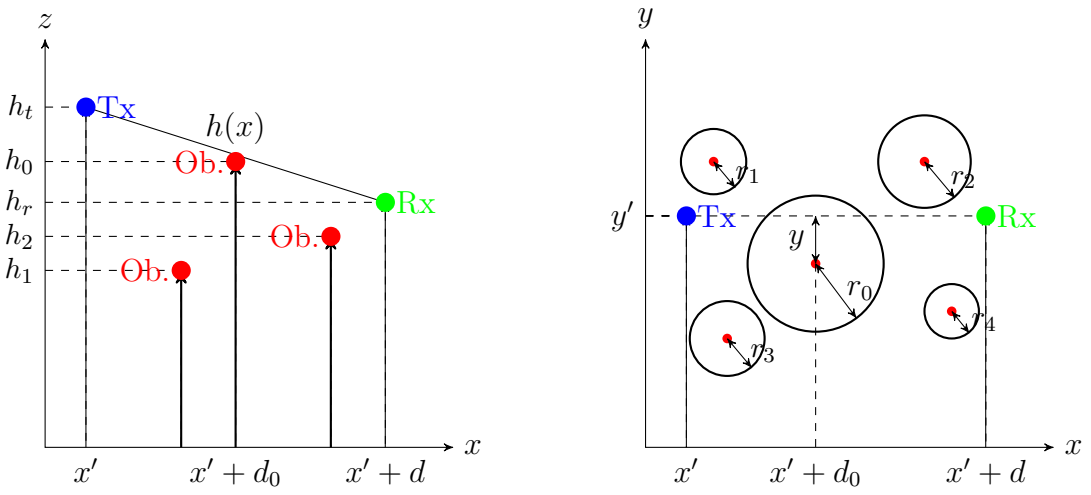

(a) Blockage due to the height of an obstacle ($xz-$plane).

(b) Blockage due to the radius of an obstacle ($xy-$plane).

Figure 4.1: A blockage event.

α_{L} and α_{N} are exponent decays experienced by the transmitted signals during LOS and NLOS communications, respectively. Then, Γ multiplies our channel matrix $\mathbf{H}$; hence, our system model is now given by:

$$\mathbf{R} = \sqrt{\rho}\Gamma\mathbf{H}\mathbf{S} + \mathbf{Z}. \tag{4.2}$$

In practical communication systems, the SNR due to NLOS communication is penalized more stringently than that due to LOS communication, i.e., $\alpha_{\mathrm{N}} > \alpha_{\mathrm{L}}$ [15].

4.2 Average PEP

The average PEP over the channel coefficients for the system in (4.2) is (cf. section 3.3):

$$\Pr\{\mathbf{S} \to \mathbf{E}|\Gamma\} = \frac{1}{2}\prod_{i=1}^{N_r}\prod_{j=1}^{r}\frac{(\widetilde{m}_j/\widetilde{\Omega})^{\widetilde{m}_j}}{\left((\rho/4)\lambda_j\Gamma + \widetilde{m}_j/\widetilde{\Omega}\right)^{\widetilde{m}_j}}. \tag{4.3}$$

Now, by averaging (4.3) over Γ, the average PEP can be written as:

$$\Pr\{\mathbf{S} \to \mathbf{E}\} = \mathbb{E}_{\Gamma}\{\Pr\{\mathbf{S} \to \mathbf{E}|\Gamma\}\}$$

$$= \frac{1}{2}\prod_{i=1}^{N_r}\prod_{j=1}^{r}\frac{(\widetilde{m}_j/\widetilde{\Omega})^{\widetilde{m}_j}}{\big((\rho/4)\lambda_j\gamma_1+\widetilde{m}_j/\widetilde{\Omega}\big)^{\widetilde{m}_j}}P_{\text{LOS}} + \frac{1}{2}\prod_{i=1}^{N_r}\prod_{j=1}^{r}\frac{(\widetilde{m}_j/\widetilde{\Omega})^{\widetilde{m}_j}}{\big((\rho/4)\lambda_j\gamma_2+\widetilde{m}_j/\widetilde{\Omega}\big)^{\widetilde{m}_j}}\big(1-P_{\text{LOS}}\big). \tag{4.4}$$

To model the effect of blockage on the diversity and coding gains, we express P_{LOS} as a function of known parameters such as the density of obstacles and their dimensions and the transceivers' locations.

4.3 Expressing P_{LOS} as a Function of Environmental Properties

We want to find P_{LOS} as a function of known environmental properties. To this end, we first find the effective density of obstacles. While the density of obstacles in the room is λ_b, not all obstacles present in a room can cause a blockage. In fact, only obstacles above a certain height and located between the transceivers can block the LOS communication, as shown in Fig. 4.1(a). Similarly, only if there exists an obstacle within a certain blocking region with a large enough diameter can there be a blockage due to its radius, as shown in Fig. 4.1(b). These two events of blockages due to heights and radii of obstacles reduce original density to an effective one. More specifically, using the Thinning Theorem from stochastic geometry [28], the effective density of obstacles λ_b' is given by:

$$\lambda_b' = \lambda_b \Pr\{\xi_1\}\Pr\{\xi_2\}, \tag{4.5}$$

where $\Pr\{\xi_1\}$ is the probability of blockage event ξ_1 due to heights of obstacles blocking the LOS link between the transceivers, and $\Pr\{\xi_1\}$ is the probability of blockage event ξ_2 due to radii of obstacles.

To find $\Pr\{\xi_1\}$, consider Fig. 4.1(a). For n obstacles in the blocking region with heights $H_1, H_2, \ldots, H_n$, $H_0 = \max\big(H_1, H_2, \ldots, H_n\big)$. From Fig. 4.1a, an obstacle with height H_0 and distance D_0 from the transmitter can block the LOS $h(x)$ if $H_0 > h(D_0)$, where $h(x)$ is

the LOS. Hence, as we show in more detail in Appendix D, $\Pr\{\xi_1\}$ is given by:

$$\begin{aligned}\Pr\{\xi_1\} &= \mathbb{E}_{D_0}\left\{\Pr\left\{H_0 > h(d_0)|D_0 = d_0\right\}\right\} \\ &= 1 - \frac{1}{(h_{\max} - h_{\min})^n}\sum_{k=0}^{n}\binom{n}{k}(h_t - h_{\min})^{n-k}\Big(\frac{h_r - h_t}{k+1}\Big)^k. \end{aligned} \tag{4.6}$$

Finding $\Pr\{\xi_2\}$, follows a similar procedure as illustrated by Fig. 4.1(b). Upon fixing d, only an object with a radius greater than $|y|$ can cause a blockage event, where y is the distance of the line perpendicularly joining the center of the blocking object to the LOS between the transceivers. For n obstacles in the blocking region with radii $R_1, R_2, \ldots, R_n$, $R_0 = \max\big(R_1, R_2, \ldots, R_n\big)$. Then, as shown in Appendix D, $\Pr\{\xi_1\}$ is given by:

$$\begin{aligned}\Pr\{\xi_2\} &= \mathbb{E}_Y\left\{\Pr\left\{R_0 > |y|\big|Y = y\right\}\right\} \\ &= 1 - \frac{1}{\big(r_{\max} - r_{\min}\big)^n}\sum_{k=0}^{n}\binom{n}{k}(-r_{\min})^{n-k}\frac{r_0^k}{k+1}. \end{aligned} \tag{4.7}$$

The volume of the blocking region is $2dh_t r_{\max}$. Thus, the number of obstacles in the blocking region is $n = \lceil 2\lambda_b dh_t r_{\max}\rceil$.

Now, to evaluate the average PEP in (4.4), we find the probability of having a LOS communication between the transceivers P_{LOS}. Let K' denote the effective number of obstacles that can cause blockage, i.e., $K' \sim \text{Poisson}(\lambda_b')$. Then, the probability of having a LOS communication is given by:

$$P_{\text{LOS}} = \Pr\left\{K' = 0\right\} = \exp\big(-\lambda_b'\big). \tag{4.8}$$

We observe from (4.4) that P_{LOS} is not a function of the SNR. And, since the diversity gain is defined in terms of the behavior of the PEP as the SNR goes to infinity, the diversity gain is not affected by the presence of obstacles. This also makes sense since the diversity gain in systems with multiple antennas is caused by the propagation of multipath components, which

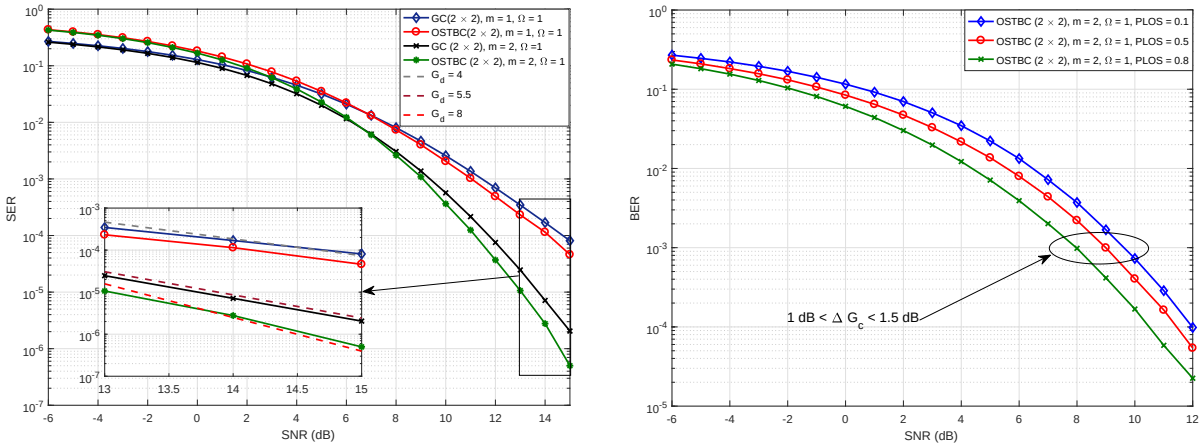

(a) OSTBC (2×2) and GC (2×2).

(b) OSTBC (2×2) with blockage.

Figure 4.2: Error performance versus SNR for space-time block codes under different Nakagami-m fading channel conditions and blockage considerations.

involve reflected paths that are not LOS, while blockage only involves obstacles obstructing LOS propagation.

By averaging the PEP, and then averaging the coding gain over Γ, we obtain:

$$G_c^b = \left\{ P_{\text{LOS}} \left(\frac{d}{d_{\text{ref}}} \right)^{-\alpha_{\text{L}}} + \left(1 - P_{\text{LOS}}\right) \left(\frac{d}{d_{\text{ref}}} \right)^{-\alpha_{\text{N}}} \right\} G_c, \tag{4.9}$$

where G_c^b is the effective coding gain when the effect of blockage is considered, and G_c is given by (3.19). We observe from (4.9) that for $\alpha_{\text{L}} = \alpha_{\text{N}} = 0$, the SNR is not reduced due to either LOS or NLOS communication. Hence, the coding gain with blockage is maximized, i.e., $G_c^b = G_c$.

4.4 Numerical Results

In this section, we simulate the error performance of space-time codes over Nakagami-m fading channels to illustrate our proposed design criteria and the effect of blockage on the diversity and coding gains. We denote the number of transmitters N_t and the time slots T (i.e., channel uses) used by a codeword as $N_t \times T$. We simulate rate-N_t OSTBCs and

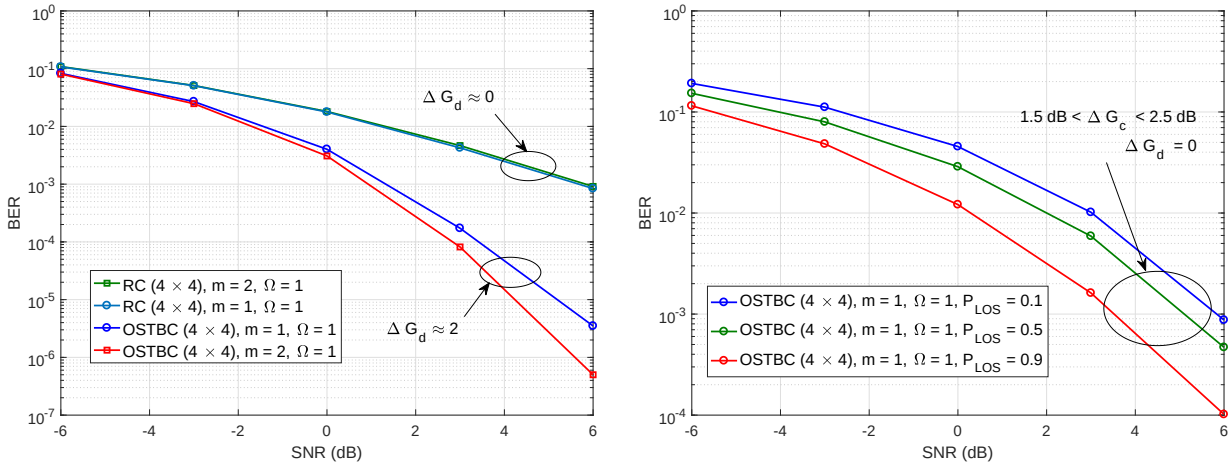

(a) OSTBC (4×4) and RC (4×4).

(b) OSTBC (4×4) with blockage.

Figure 4.3: BER versus SNR for space-time block codes under different Nakagami-m fading channel conditions and blockage considerations.

NOSTBCs and the full-rate golden code (GC).

Figure 4.2(a) shows the symbol error rate (SER) for the OSTBC (2×2), which is the Alamouti code [6], and the golden code (GC) (2×2) [41] over the Nakagami-m fading channel. The modulations used are BPSK and QPSK for the GC (2×2) and the OSTBC (2×2), respectively. This choice of modulations is to normalize the transmission rates in bits per channel use for each scheme since the GC (2×2) is full-rate and the OSTBC (2×2) is rate-1, i.e., now both schemes transmit at the same rate of 2 bits per channel use. When $m = 1$, i.e., Rayleigh fading, both the OSTBC (2×2) and the GC (2×2) achieve the full diversity of $N_t N_r$, which is 4 in this case. However, when the fading severity is reduced, i.e., $m = 2$, the OSTBC (2×2) achieves the full diversity of mN_tN_r, which is 8, while is GC (2×2) only achieves a diversity gain of about 5.5. Note that, when $m = 2$, the worst-case $\widetilde{m}_j$ for the OSTBC (2×2) is 2, resulting in an achievable diversity gain of 8, and the worst-case $\widetilde{m}_j$ the GC (2×2) is 1.333, resulting in a minimum achievable diversity gain of about 5.332. Hence, the reason why orthogonal codes are able to achieve the maximum diversity order of $N_t N_r m_{\max}$ is that they produce a unitary matrix $\mathbf{U}$ that is the identity, as derived in Sec. 3.4. On the other hand, while the GC (2×2) achieves full-diversity over Rayleigh fading

channels [41], it does not necessarily result in a $\mathbf{U}$ whose columns are permutations of those of the identify; hence, it does not achieve full diversity over Nakagami-m fading channels.

In Fig. 4.2(b), we simulate the bit error rate (BER) of the OSTBC (2×2) when blockage is incorporated into the channel model. The simulated scenario uses values for α_{L} and α_{N} in [15] for 60 GHz and $\gamma_1 = 0.9$ and $\gamma_2 = 0.5$. Varying the density λ_b changes P_{LOS} as given by (4.2)–(4.8). We observe from Fig. 4.2(b) that increasing the probability of a LOS communication does not affect the slope of the BER versus SNR curve but shifts the curve to the left. We represent this shift in the BER curve by ΔG_c. For a BER of 10^{-3}, Reducing P_{LOS} from 0.8 to 0.5 and 0.1 shifts the BER curve to left by 1.5 dB and 1 dB, respectively. That is, the coding gain which is represented by translations of the BER curve along the SNR axis is influenced by blockage, while the diversity gain which represented by the slope is not, conforming with our analysis in Sec. III.

We repeat our simulation for a higher number of transmit and receive antennas as shown in Figures 4.3. Specifically, we simulated a simple repetition code (RC) (4×4) with four transmit and receive antennas and the OSTBC (4×4) proposed in [19, eq. (4)], i.e., the codeword $\mathcal{D}_{4\times4}$ in [5, eq. (7.51)]. Figure 4.3(a) shows that even for a larger number of transmit antennas, a simple RC is unable to improve the diversity gain as we reduce the severity of fading, i.e., as m is doubled. On the other hand, as shown in Fig. 4.3(a), the OSTBC (4×4) is able to approximately double the diversity gain as we double the value of m. A BER of 10^{-3} is achieved at 3.5 dB for a P_{LOS} of 0.9. As P_{LOS} decreases to 0.5 and 0.1, the BER of 10^{-3} is achieved at about 5 dB and 6 dB, respectively. But, changing As P_{LOS} does not affect the slopes of BER curves. Thus, the coding gain is affected by blockage, but the diversity gain is not. Hence, our design criteria are illustrated to hold for a larger number of transmit antennas as well. Furthermore, increasing P_{LOS} results only in a shift in the BER curve to the left, increasing the coding gain, and does not affect the diversity gain (slope of the BER curve), as shown in Fig. 4.3(b).

Note that antenna arrays with a large number of antennas at millimeter-wave frequencies

can be used to electronically steer main-lobes. But, the benefits in terms of diversity and coding gains are only achieved due to signals traveling through independent paths via multiple antennas. For instance, utilizing two main antenna arrays at the transmitter and receiver such that each has an independent main-lobe corresponds to the simulations for the 2×2 system provided. Hence, when a large number of antennas is used in antenna arrays, it is important to consider the number of independent main-lobes when designing for particular coding and diversity gains rather than the number of antennas in each antenna array.

CHAPTER 5

Conclusions and Future Works

In the first part of this thesis, we showed that the Nakagami-m fading distribution can accurately model the statistics of small-scale fading in indoor environments at 60 GHz. To this end, we simulated the CTF as a function of environmental properties of the room and the locations of the transmitter and receiver. This allowed us to obtain an empirical distribution of the CTF. We were then able to best-fit the obtained empirical distribution with analytical distributions. This led us to conclude that the Nakagami-m-distributed amplitudes and uniformly-distributed phases accurately model the statistics of the CTF. As expected, the Rayleigh distribution is not a good fit for the statistics of the CTF. The Rician distribution was a good fit, but the Nakagami-m distribution was the best fit in terms of average mean squared error.

In the second part of this thesis, assuming the channel coefficients modeling small-scale fading are complex random variables with Nakagami-m-distributed amplitudes and uniformly distributed phases, we derived an upper bound on the PEP that well-describes the diversity and coding gains. This allowed us to provide design criteria for maximizing the diversity and coding gains over MIMO Nakagami-m fading channels. This included new interesting properties of space-time codes to maximize these gains, which do not necessarily apply in conventional Rayleigh and Rician fading channels. For instance, the maximum diversity gain of $rN_t m_{\max}$ is achievable by space-time block codes that result in a unitary matrix $\mathbf{U}$ whose columns are permutations of those of the identity matrix. Otherwise, space-time codes that produce a matrix $\mathbf{U}$ that has at least two non-zero entries along the same column (or row) achieve a diversity gain strictly less than $rN_t m_{\max}$. Furthermore, we showed that there is a trade-off between the diversity and coding gains. We also studied the effect of blockage due to humans and other objects on the PEP. Our analysis and simulations show that blockage results only in a shift of the BER versus SNR curve (i.e., affects coding gain), and does not affect the slope of the BER curve (i.e., does not affect the diversity gain). We expressed the

reduction in the coding gain as a function of the probability of a LOS communication, path loss exponents, the distance between transceivers, and the density of obstacles.

The following are interesting research directions and possible extensions of this work.

- The design of space-time codes that satisfy the design criteria proposed and are optimized for Nakagami-m fading channels is an appealing research problem.
- Derivation of design criteria for MIMO Nakagami-m fading channels when the channel matrix is known at the transmitter.
- Derivation of design criteria for generalized fading channels.
- Analysis of average error performance when space-time codes are used in millimeter-wave cellular networks.
- Analysis of the diversity and coding gains when the receiver implements sub-optimal, but more computationally efficient, decoding methods such as the linear minimum mean square error and the zero-forcing decoders.
- Performing further measurements at millimeter-wave frequencies in indoor and outdoor environments to obtain more accurate channel models.

Appendix A: Normalization Convention

In this appendix, we describe the normalization convention used throughout this paper. In particular consider the system model assumed:

$$\mathbf{R} = \mathbf{HS} + \mathbf{Z}, \tag{5.1}$$

where $\mathbf{S} = [s_{i,j}] \in \mathbb{C}^{N_t \times T}$ is the normalized transmitted symbols matrix; $\mathbf{H} = [h_{i,j}] \in \mathbb{C}^{N_r \times N_t}$ is the normalized channel matrix; $\mathbf{Z} = [z_{i,j}] \in \mathbb{C}^{N_r \times T}$ is the normalized complex additive white Gaussian noise (AWGN) matrix, i.e., $z_{i,j} \sim \mathcal{CN}(0,1)$; and $\rho \in [0, \infty)$ is the average SNR at the transmitter.

Then, from (5.1) the entry $r_{i,j}$ of $\mathbf{R}$ can be written as:

$$r_{i,j} = \sqrt{\rho} \sum_{j=1}^{N_t} h_{i,j} s_{j,i} + z_{i,j}, \qquad \text{for } i = 1, \ldots, N_r, \text{ and } j = 1, \ldots, T. \tag{5.2}$$

The normalization makes sure that the transmitter adheres to power a budget such that the signal to noise ratio in (5.2) is ρ, i.e.,

$$\rho = \frac{\mathbb{E}\{|\sqrt{\rho} \sum_{j=1}^{N_t} h_{i,j} s_{j,i}|^2\}}{\mathbb{E}\{|z_{i,j}|^2\}} \tag{5.3}$$

$$\overset{\text{(a)}}{=} \frac{\rho \sum_{j=1}^{N_t} \mathbb{E}\{|h_{i,j}|^2\} \, \mathbb{E}\{|s_{j,i}|^2\}}{\mathbb{E}\{|z_{i,j}|^2\}}, \tag{5.4}$$

where (a) follows from the fact that $h_{i,j}$'s are independent of each other and of $s_{j,i}$'s. For (5.4) to hold, we dictate that $\mathbb{E}\{|h_{i,j}|^2\} = 1$, $\mathbb{E}\{|s_{j,i}|^2\} = 1/N_t$, and $\mathbb{E}\{|z_{i,j}|^2\} = 1$. Therefore, normalized $\mathbf{H}$, $\mathbf{S}$, and $\mathbf{Z}$, have entries that satisfy the power power budget constraint in (5.4).

Appendix B: Proof of PDF of $\beta_{i,j}$

Consider the complex Nakagami-m random variable $X_i = R_i \exp(-j\phi_i)$, where $R_i \sim$ Nakagami(m_i, Ω_i), $\phi_i \sim U(-\pi, \pi)$, R_i's are independent and ϕ_i's are independent, the amplitudes R_i's and the phases ϕ_i's are independent, and $1 \leq i \leq n$. The envelope $|W|$ of the sum of complex Nakagami-m independent random variables is defined as:

$$|W| = \left| \sum_{i=1}^{n} X_i \right|. \tag{5.5}$$

Then, using the method in [20, 21], $W \sim$ Nakagami(m', Ω'), where:

$$\Omega' = \sum_{i=1}^{n} \Omega_i \tag{5.6}$$

$$m' = \frac{\left(\sum_1^n \Omega_i \right)^2}{\sum_{i=1}^{n} \frac{\Omega_i^2}{m_i} + \sum_{i=1}^{n} \sum_{\substack{j=1 \\ j \neq i}}^{n} \Omega_i \Omega_j}. \tag{5.7}$$

To use this method to find the PDF of $\beta_{i,j} \triangleq \sum_{j'=1}^{N_t} u_{j',j} h_{i,j'}$, where $|h_{i,j'}| \sim$ Nakagami(m, Ω) and $\angle h_{i,j'} \sim U(-\pi, \pi)$, we note that using a simple algebraic manipulation the PDF of each term $u_{j',j} h_{i,j'} \sim$ Nakagami$(m, |u_{j',j}|^2 \Omega)$. Hence, via applying (5.7), the PDF of $|\beta_{i,j}| \sim$ Nakagami$(\widetilde{m}_j, \widetilde{\Omega})$, where:

$$\widetilde{\Omega} = \sum_{i=1}^{i=N_t} |u_{j',j}|^2 \Omega = \Omega \tag{5.8}$$

$$\widetilde{m}_j = \frac{\left(\sum_{j'=1}^{N_t} |u_{j',j}|^2 \Omega \right)^2}{\sum_{j'=1}^{N_t} \frac{|u_{j',j}|^4 \Omega^2}{m} + \sum_{j'=1}^{N_t} \sum_{\substack{j''=1 \\ j'' \neq j'}}^{N_t} |u_{j',j}|^4 \Omega^2} \tag{5.9}$$

$$= \frac{m}{\sum_{j'=1}^{N_t} |u_{j',j}|^4 + m \sum_{j'=1}^{N_t} \sum_{\substack{j''=1 \\ j'' \neq j'}}^{N_t} |u_{j',j}|^2 |u_{j'',j}|^2}. \tag{5.10}$$

Appendix C: Proof of Proposition 1: The Bounds on the Coding Gain

The upper on G_c is obtained as follows. Since $\log(\cdot)$ is concave function, we can equivalently maximize G_c in (3.19) as:

$$\begin{aligned}
&\max\left\{\log\left(\frac{\Omega}{4}\prod_{j=1}^{r}\left(\frac{\lambda_j}{\widetilde{m}_j}\right)^{\frac{\widetilde{m}_j}{\sum_{j=1}^{r}\widetilde{m}_j}}\right)\right\}\\
=&\max\left\{\frac{\Omega}{4}\sum_{j=1}^{r}\frac{\widetilde{m}_j}{\sum_{j=1}^{r}\widetilde{m}_j}\log\left(\frac{\lambda_j}{\widetilde{m}_j}\right)\right\}\\
=&\max\left\{\frac{\Omega}{4}\,\mathbb{E}_X\left\{-\log(X)\right\}\right\},
\end{aligned}\tag{5.11}$$

where $X \triangleq \widetilde{m}_j/\lambda_j$, and its probability mass density (PMF) is $\Pr\left\{X=\dfrac{\widetilde{m}_j}{\lambda_j}\right\}=\dfrac{\widetilde{m}_j}{\sum_{j=1}^{r}\widetilde{m}_j}$. The expression in (5.11) can be seen as an entropy maximization problem. It is well-known that the discrete uniform distribution maximizes entropy [32]. Hence, (5.11) is maximized when $\Pr\left\{X=\dfrac{\widetilde{m}_j}{\lambda_j}\right\}=\dfrac{\widetilde{m}_j}{\sum_{j=1}^{r}\widetilde{m}_j}=p,\ \forall j=1,\ldots,N_t$, and $p\in[0,1]$. To solve for p, we observe that all $\widetilde{m}_j$'s are the same due to the fact that the uniform PMF maximizes entropy. Therefore, $p=\dfrac{1}{r}$, and the maximum coding gain is obtained when $\widetilde{m}_j=m_{\min}$, i.e.,:

$$\max\left\{\frac{\Omega}{4}\,\mathbb{E}_X\left\{-\log(X)\right\}\right\}=\frac{\Omega}{4}\sum_{j=1}^{r}\frac{1}{r}\log\left(\frac{\lambda_j}{m_{\min}}\right).\tag{5.12}$$

Similarly, to minimize G_c a similar procedure is followed where the dummy random variable is defined as $X\triangleq\dfrac{\lambda_j}{\widetilde{m}_j}$. Then, the minimum G_c would be obtained when $\Pr\left\{X=\dfrac{\lambda_j}{\widetilde{m}_j}\right\}=\dfrac{\widetilde{m}_j}{\sum_{j=1}^{r}\widetilde{m}_j}=p,\ \forall j=1,\ldots,N_t$. Since all $\widetilde{m}_j$'s are the same, the minimum is obtained when $\widetilde{m}_j=M_{\max}$, i.e., the minimum coding gain is given by:

$$\min\left\{\frac{\Omega}{4}\sum_{j=1}^{r}\frac{\widetilde{m}_j}{\sum_{j=1}^{r}\widetilde{m}_j}\log\left(\frac{\lambda_j}{\widetilde{m}_j}\right)\right\}=\frac{\Omega}{4}\sum_{j=1}^{r}\frac{1}{r}\log\left(\frac{\lambda_j}{m_{\max}}\right).\tag{5.13}$$

Appendix D: Evaluating the probability of blockage due to heights and radii of obstacles

We find expressions for $\Pr\{\xi_1\}$ and $\Pr\{\xi_1\}$, which are the probabilities of blockage events due to the heights and radii of obstacles, respectively. From Fig. 4.1(a), a blockage event due to the height of an obstacles occurs if H_0 is greater than $h(D_0)$, where H_0 is the maximum height of the obstacles in the blocking region, i.e.,for n obstacles in the blocking region with heights $H_1, H_2, \ldots, H_n$, $H_0 = \max\big(H_1, H_2, \ldots, H_n\big)$. Hence, the probability of blockage due to heights of obstacles is given by:

$$\begin{aligned}
\Pr\{\xi_1\} &= \Pr\Big\{h_0 > h(D_0)\Big\} \\
&= 1 - \mathbb{E}_{D_0}\left\{F_{H_0|D_0=d_0}\Big(\frac{(h_t-h_r)}{d}D_0 + h_t\Big)\right\} \\
&= \begin{cases} 0 & h(D_0) \geq h_{\max} \\ \mathbb{E}_{D_0}\left\{\dfrac{\frac{(h_t-h_r)}{d}D_0 + h_t - h_{\min}}{h_{\max}-h_{\min}}\right\}^n & h_{\min} \leq h(D_0) < h_{\max} \\ 1 & h(D_0) < h_{\min}. \end{cases}
\end{aligned}$$

Now, evaluating (4.6) for $h_{\min} \leq h(D_0) < h_{\max}$, using the fact that $D_0 \sim U(0,d)$, and using the binomial theorem, we obtain:

$$\begin{aligned}
&\Pr\{\xi_1\} \\
&= 1 - \int_0^d \left\{\frac{\frac{(h_t-h_r)}{d}d_0 + h_t - h_{\min}}{h_{\max}-h_{\min}}\right\}^n dd_0 \\
&\overset{(a)}{=} 1 - \frac{1}{(h_{\max}-h_{\min})^n}\sum_{k=0}^{n}\binom{n}{k}(h_t-h_{\min})^{n-k}\Big(\frac{h_r-h_t}{k+1}\Big)^k,
\end{aligned}$$

where n is the number of obstacles in the blocking region and is equal to $\lceil \lambda_b d h_t r_{\max} \rceil$ and (a) follows from the binomial expansion of the integrand.

Finding $\Pr\{\xi_2\}$ follows a similar procedure. From Fig. 4.1(b), the starting point of the proof is $\Pr\{\xi_2\} = \Pr\{R_0 > |y|\}$, where R_0 is the radius of the widest obstacle in the blocking region, i.e., $R_0 = \max\big(R_1, R_2, \ldots, R_n\big)$. The rest follows as in the previous derivation to obtain

$$\begin{aligned}\Pr\{\xi_2\} &= \mathbb{E}_Y\left\{\Pr\left\{R_0 > |y|\big|Y = y\right\}\right\} \\ &= 1 - \frac{1}{\big(r_{\max} - r_{\min}\big)^n}\sum_{k=0}^{n}\binom{n}{k}(-r_{\min})^{n-k}\frac{r_0^k}{k+1}.\end{aligned}$$

Bibliography

[1] V. Tarokh, N. Seshadri, and A. R. Calderbank, "Space-time codes for high data rate wireless communication: performance criterion and code construction," *IEEE Transactions on Information Theory*, vol. 44, no. 2, pp. 744–765, Mar. 1998.

[2] A. Maltsev, R. Maslennikov, A. Sevastyanov, A. Khoryaev, and A. Lomayev, "Experimental investigations of 60 GHz wlan systems in office environment," *IEEE Journal on Selected Areas in Communications*, vol. 27, no. 8, 2009.

[3] T. S. Rappaport, S. Sun, R. Mayzus, H. Zhao, Y. Azar, K. Wang, G. N. Wong, J. K. Schulz, M. Samimi, and F. Gutierrez, "Millimeter wave mobile communications for 5G cellular: It will work!" *IEEE access*, vol. 1, pp. 335–349, 2013.

[4] A. S. Tanenbaum, *Structured computer organization*. Pearson Education India, 2016.

[5] J. R. Hampton, *Introduction to MIMO communications*. Cambridge university press, 2013.

[6] S. M. Alamouti, "A simple transmit diversity technique for wireless communications," *IEEE Journal on Selected Areas in Communications*, vol. 16, no. 8, pp. 1451–1458, Oct. 1998.

[7] V. Nurmela, A. Karttunen, A. Roivainen, L. Raschkowski, V. Hovinen, J. Y. EB, N. Omaki, K. Kusume, A. Hekkala, R. Weiler *et al.*, "Deliverable d1. 4 metis channel models," *Mobile Wireless Commun. Enablers Twenty-Twenty Inf. Soc.(METIS)*, 2014.

[8] M. K. Samimi and T. S. Rappaport, "3-D millimeter-wave statistical channel model for 5G wireless system design," *IEEE Transactions on Microwave Theory and Techniques*, vol. 64, no. 7, pp. 2207–2225, 2016.

[9] "FCC, millimeter wave 70/80/90 GHz service," https://www.fcc.gov/wireless/bureau-divisions/broadband-division/millimeter-wave-708090-ghz-service, accessed: 2017.

[10] K. Venugopal, M. C. Valenti, and R. W. Heath, "Device-to-device millimeter wave communications: Interference, coverage, rate, and finite topologies," *IEEE Transactions on Wireless Communications*, vol. 15, no. 9, pp. 6175–6188, 2016.

[11] T. Bai and R. W. Heath, "Coverage and rate analysis for millimeter-wave cellular networks," *IEEE Transactions on Wireless Communications*, vol. 14, no. 2, pp. 1100–1114, 2015.

[12] V. Vakilian, H. Mehrpouyan, Y. Hua, and H. Jafarkhani, "High-rate space coding for reconfigurable 2x2 millimeter-wave MIMO systems," *arXiv preprint arXiv:1505.06466*, 2015.

[13] N. Eshraghi, B. Maham, and V. Shah-Mansouri, "Outage probability analysis of the millimeter-wave relaying systems," in *Personal, Indoor, and Mobile Radio Communications (PIMRC), 2016 IEEE 27th Annual International Symposium on*. IEEE, 2016, pp. 1–5.

[14] B. Makki, T. Svensson, M. Brandt-Pearce, and M.-S. Alouini, "On the performance of millimeter wave-based RF-FSO multi-hop and mesh networks," *arXiv preprint arXiv:1703.09298*, 2017.

[15] P. F. Smulders, "Statistical characterization of 60-GHz indoor radio channels," *IEEE Transactions on Antennas and Propagation*, vol. 57, no. 10, pp. 2820–2829, 2009.

[16] J. Hansen, "A novel stochastic millimeter-wave indoor radio channel model," *IEEE Journal on Selected Areas in Communications*, vol. 20, no. 6, pp. 1240–1246, 2002.

[17] J. Hansen and M. Nold, "Analytic calculation of the power delay profile for single room wireless lan environments," in *Global Telecommunications Conference, 2000. GLOBECOM'00. IEEE*, vol. 1. IEEE, 2000, pp. 98–102.

[18] D. Steinmetzer, J. Classen, and M. Hollick, "MmTrace: modeling millimeter-wave indoor propagation with image-based ray-tracing," in *Computer Communications Workshops (INFOCOM WKSHPS), 2016 IEEE Conference on*. IEEE, 2016, pp. 429–434.

[19] V. Tarokh, H. Jafarkhani, and A. R. Calderbank, "Space-time block codes from orthogonal designs," *IEEE Transactions on Information Theory*, vol. 45, no. 5, pp. 1456–1467, Jul. 1999.

[20] M. Nakagami, "The m-distribution-a general formula of intensity distribution of rapid fading," *Statistical Method of Radio Propagation*, pp. 3–34, 1960.

[21] Z. Du, J. Cheng, and N. C. Beaulieu, "Accurate error-rate performance analysis of OFDM on frequency-selective nakagami-m fading channels," *IEEE Transactions on Communications*, vol. 54, no. 2, pp. 319–328, Feb. 2006.

[22] A. Aboutaleb, W. Fatnassi, Z. Rezki, and A. Chaaban, "Error performance of space-time codes over MIMO millimeter-wave channels: Design criteria and new insigths," *Submitted to Transactions on Comunications*, April 2018.

[23] Y. J. Chun, S. L. Cotton, H. S. Dhillon, A. Ghrayeb, and M. O. Hasna, "A stochastic geometric analysis of device-to-device communications operating over generalized fading channels," *IEEE Transactions on Wireless Communications*, vol. 16, no. 7, pp. 4151–4165, July 2017.

[24] S. A. Ali, N. S. Kambo, and E. Aliriza, "Exact expression and tight bound on pairwise error probability for performance analysis of turbo codes over nakagami-m fading channels," *IEEE Communications Letters*, vol. 11, no. 5, pp. 399–401, May 2007.

[25] A. Maaref and S. Aissa, "Performance analysis of orthogonal space-time block codes in spatially correlated MIMO nakagami fading channels," *IEEE Transactions on Wireless Communications*, vol. 5, no. 4, pp. 807–817, Apr. 2006.

[26] M. D. Renzo, "Stochastic geometry modeling and analysis of multi-tier millimeter wave cellular networks," *IEEE Transactions on Wireless Communications*, vol. 14, no. 9, pp. 5038–5057, Sep. 2015.

[27] M. R. Akdeniz, Y. Liu, M. K. Samimi, S. Sun, S. Rangan, T. S. Rappaport, and E. Erkip, "Millimeter wave channel modeling and cellular capacity evaluation," *IEEE Journal on Selected Areas in Communications*, vol. 32, no. 6, pp. 1164–1179, Jun. 2014.

[28] S. N. Chiu, D. Stoyan, W. S. Kendall, and J. Mecke, *Stochastic geometry and its applications*. John Wiley & Sons, 2013.

[29] S. Singh, M. N. Kulkarni, A. Ghosh, and J. G. Andrews, "Tractable model for rate in self-backhauled millimeter wave cellular networks," *IEEE Journal on Selected Areas in Communications*, vol. 33, no. 10, pp. 2196–2211, Oct. 2015.

[30] A. Aboutaleb, W. Fatnassi, Z. Rezki, and A. Chaaban, "On the error performance of space-time codes over MIMO nakagami fading channels with blockage," *Submitted to Biennial Symposium on Communications 2018 (BSC 2018)*, April 2018.

[31] K. D. P. Dharmawansa and R. M. A. P. Rajatheva, "On the pairwise error probability bounds of sttc over nakagami-m fading channels," in *Proc. IEEE Int. Conf. Communications ICC 2005*, vol. 5, May 2005, pp. 2927–2931 Vol. 5.

[32] A. Goldsmith, *Wireless communications*. Cambridge university press, 2005.

[33] H. Jafarkhani, *Space-time coding: theory and practice*. Cambridge university press, 2005.

[34] W. Jarosz, *Efficient Monte Carlo methods for light transport in scattering media*. University Of California, San Diego, 2008.

[35] P. Almers, E. Bonek, A. Burr, N. Czink, M. Debbah, V. Degli-Esposti, H. Hofstetter, P. Kyösti, D. Laurenson, G. Matz *et al.*, "Survey of channel and radio propagation models for wireless MIMO systems," *EURASIP Journal on Wireless Communications and Networking*, vol. 2007, no. 1, pp. 56–56, 2007.

[36] "Mathworks, mle (maximum likelihood estimator)," https://www.mathworks.com/help/stats/mle, accessed: 2017.

[37] A. A. M. Saleh and R. Valenzuela, "A statistical model for indoor multipath propagation," *IEEE Journal on Selected Areas in Communications*, vol. 5, no. 2, pp. 128–137, Feb. 1987.

[38] S. H. Chang, P. C. Cosman, and L. B. Milstein, "Chernoff-type bounds for the gaussian error function," *IEEE Transactions on Communications*, vol. 59, no. 11, pp. 2939–2944, Nov. 2011.

[39] P. Dharmawansa, N. Rajatheva, and K. Ahmed, "On the distribution of the sum of nakagami-m random variables," *IEEE Transactions on Communications*, vol. 55, no. 7, pp. 1407–1416, Jul. 2007.

[40] I. S. Gradshteyn and I. M. Ryzhik, *Table of integrals, series, and products*. Academic press, 2014.

[41] F. Oggier, G. Rekaya, J. C. Belfiore, and E. Viterbo, "Perfect space-time block codes," *IEEE Transactions on Information Theory*, vol. 52, no. 9, pp. 3885–3902, Sept 2006.